Empirical Star Formation Estimates in Galaxy Evolution

by

Nityasri Mandyam Doddamane

A dissertation submitted in partial fulfillment

of the requirements for the degree of

Doctor of Philosophy

Department of Physics

New York University

January, 2019

Michael R. Blanton

© Nityasri Mandyam Doddamane
all rights reserved, 2019

Abstract

One of the crucial unsolved puzzles in astronomy has been the question of how galaxies end the process of star formation. A key piece in this puzzle is figuring out how to robustly infer star formation rates and the cosmic star formation histories of galaxies from observed photometric and spectroscopic data. The star formation history of a galaxy is encoded in its spectrum, which can be thought of as a fingerprint of a galaxy. However, spectroscopic information is often unavailable as it is more expensive to obtain. And where available, it can be limited in terms of interpretability by the dependence on the fiber diameter used and the physical properties of the galaxy in question.

The class of techniques known as SED (Spectral Energy Distribution) fitting tackles this problem by inferring the spectrum of a galaxy from photometric and spectroscopic data. Over the last decade, SED-fitting methods have become increasingly more sophisticated both in terms of model predictions as well as accounting for effects of more complex physical mechanisms such as dust absorption/emission. Another significant development, has been the rapidly growing field of IFU (Integral Field Unit) spectroscopy with a view to obtaining spatially resolved spectra with high S/N ratio of galaxies. With the advent of ongoing surveys such as MaNGA (Mapping Nearby Galaxies at Apache Point Observatory), the largest IFU-based survey thus far, we are better poised to answer this question than ever

before.

In this dissertation, I examine these two techniques for estimating star formation histories. First, using data from NASA Sloan Atlas (NSA) catalog along with the Wide-field Infrared Survey (WISE), I compare star formation rates obtained from two different methods: one, a UV-to-IR SED fitting method that accounts for dust and the other, a purely UV photometry-based approach. Using galaxy environments as a third independent parameter, I find a population of dust obscured star formers that masquerade as much lower star formation galaxies when only UV-optical information is available, but which live in the same large scale environments as other star forming galaxies.

In the second part, I examine the robustness of star formation history measurements from one of the largest available and most influential catalogs available, the Sloan Digital Sky Survey (SDSS) Legacy Survey. This catalog is limited by the fact that it uses small aperture fibers (3 arcsecond diameter) to measure galaxies that can sometimes have much larger angular extent. Spatially resolved spectroscopy from MaNGA measures galaxies more completely, but for a much smaller sample. I use aperture measurements of key spectral indicators of age, stellar mass and star formation history such as the $H\delta_{\rm A}$ absorption line index and the $D_{\rm n}4000$ break to quantify the effects of the small fiber aperture on the Legacy Survey sample results. From these results I show that biases exist in the measurements of stellar mass from the SDSS Legacy Survey, but that for most galaxies these biases are small.

Contents

Listing of figures

For Srikar.

Acknowledgments

Here's where I acknowledge a lot of people.

... As for me, nothing in the universe can be the same if somewhere, no one knows where, a sheep we never saw has or has not eaten a rose.... Look up at the sky. Ask yourself, "Has the sheep eaten the flower or not?" And you'll see how everything changes.... And no grown-up will ever understand how such a thing could be so important!

Antoine de Saint-Exupêry (The Little Prince)

0 Introduction

0.1 A Brief History of Galaxy Evolution

0.1.1 The Discovery of Galaxies

One of the momentous shifts in scientific thinking was the realization that our Sun might be one of many stars in the Universe. From this sprung the idea that perhaps the gravitationally bound system of stars, stellar remnants, gas and dust that the Sun is a part of is one

of many such structures known as galaxies. The bright band of stars and dust that we observe in the night sky, which we now know as our own galaxy, the Milky Way, has been a puzzling topic since ancient times. The Greek philosopher Democritus is known to have speculated that this might be a band of distant stars but the thought was left by the wayside with the advent of Aristotelian physics. The astronomers of medieval Islam, such as Alhazen, al-Biruni and Ibn-Bajjah, centuries later, also hypothesized that the Milky Way was made of many stars such as our own Sun. However, observational proof for this came only in the 17th century when the Italian astronomer, Galileo Galelei pointed his telescope at this band and confirmed that the Milky Way was indeed made up of a huge number of faint stars.

Since the debate on a geocentric versus heliocentric Universe was still ongoing, Galileo's observations weren't given credence until more than century later, during which time, the development of Keplerian orbital mechanics and Newtonian Theory of Gravitation had resulted in a successful explanation of the Solar System and its dynamics. The idea that the galaxy might be a rotating configuration of a huge number of stars held together by gravitational forces that contained smaller gravitationally bound configurations such as our Solar System was first theorized by the English astronomer, Thomas Wright, in 1750. On the heels of his observation that the faint (then so-called) "nebulae" observed might be distant galaxies that came out of "external creations", philosopher Immannuel Kant hypothesized the existence of many such "island Universes" and speculated that these could potentially form and evolve independently from our own, thus laying the underpinnings of the study of galaxy formation and evolution.

0.1.2 Early Studies of Galaxies

William Herschel, in the 1780s, surveyed the stars in the Milky Way in multiple directions and discovered that the density of stars was greater on one side than the other. One of the earliest catalogues of galaxy-like objects was developed by Charles Messier, also towards the end of the 18th century, following which William Herschel assembled a catalog of 5000 nebulae. In the 19th century, with advances in optics and instrumentation, the first telescope to distinguish between elliptical and spiral galaxies was built by Lord Rosse. Additionally, this telescope could resolve point sources within the nebulae, thus confirming that galaxies were indeed "island universes" as Wright and Kant had surmised.

In early 20th century, astronomers were beginning to get interested in the chemical composition of these nebulae and started recording their spectra. With the advent of Einstein's Special Theory of Relativity, one could calculate the radial velocity of a "nebula" based on how its spectrum is Doppler-shifted. And so it happened that the American astronomer, Vesto Slipher, became the first person to measure galactic redshifts in 1912. While studying the chemical composition of bright spiral nebulae, he noticed that they were all highly Doppler-shifted, with estimated radial velocities that were much higher than the velocities of stars in the Milky Way. He also noticed that there were more "red-shifted" (i.e. moving away from us) nebulae than "blue-shifted" ones, an observation that would later propel Edwin Hubble to propose that the Universe was expanding.

In the 1920s, a series of observations made by Edwin Hubble, Ernst Opik, etc., confirmed that Andromeda was not a part of the Milky Way and was a galaxy is its own right, thus effectively settling the "Great Debate" of the times and confirming that our galaxy was just one of many galaxies in the Universe. Georges Lemaítre, a Belgian physicist, predicted, on

theoretical grounds rooted in Einstein's General Theory of Relativity, that the redshifts of galaxies should increase with distance. In 1929, Edwin Hubble looked at the distances and velocities of 46 galaxies and observed the same (Hubble, 1929): that their radial velocities increased with distance from us, thus theorizing what we know today as Hubble's Law (or alternately, the Hubble-Lemaítre Law). Edwin Hubble further analyzed the morphologies of these galaxies and came up with the Hubble Sequence, a classification of galaxy morphology (Fig. 1). The Swiss astrophysicist, Fritz Zwicky, in 1933, while studying galaxy clusters, noticed that the orbits of the galaxies were not accounted for by the mass of its luminous components, leading him to believe that there must be some "missing" mass (Zwicky, 1937) that does not interact electromagnetically, thus remaining unseen and termed it *dunkle Materie*, i.e.,"dark matter".

Thus with the emergence of new theories of spacetime, an expanding Universe that (as it was termed later) began with a "big bang", the existence of matter that doesn't interact electromagnetically, the study of galaxies in the 1930s set in motion a paradigm shift for astronomy and cosmology. The new questions were: How were the earliest galaxies formed? What would explain the diversity in morphologies seen in galaxies today? Is the Universe set to expand indefinitely? What drives the expansion of the Universe? What is dark matter? If the Universe's origins were homogeneous, how do we explain the heterogenous nature of the populations of galaxies seen?

0.1.3 Galaxy Evolution and Cosmology

The explorations in the latter half of the 20th century confirmed a few of the hypotheses discussed above, along with answering a few of those questions. In the 1960s and 1970s,

Vera Rubin, Kent Ford, and Ken Freeman analyzed rotation curves of spiral galaxies and provided strong evidence for the existence of dark matter (Freeman, 1970). Rubin inferred that most galaxies contain around six times as much dark matter as visible mass (Rubin et al., 1980), thus placing new constraints on galaxy formation and evolution in the Universe.

The two predominant theories of the origin of the Universe were: the "Big Bang Theory", originally proposed by Georges Lemaítre, and the "Steady State Theory" (essentially an unchanging Universe whose density remains the same in spite of expansion due to continuous creation of matter) proposed by Fred Hoyle. However, with theories of Big Bang Nucleosynthesis (the $\alpha\beta\gamma$ paper; Alpher et al. 1948) that successfully explained how the elements of the of the Universe came to be formed after the Big Bang and radio source counts which were also correctly accounted for by the Big Bang Theory swung cosmologists to favor this over the Steady State Theory. The final nail in the coffin was the successful detection of the Cosmic Microwave Background (CMB), predicted by the Big Bang Theory (Penzias & Wilson, 1965). According to the Big Bang Theory, the early Universe cools from a very hot state and remains an ionized plasma for the first few hundred thousand years (until redshift $z \sim 1100$). The emission from this era should be a Planck spectrum of the plasma at about the time that hydrogen recombines, redshifted due to the universe's expansion since then. This model predicts a spectrum peaking at near microwave wavelengths today, and the CMB is indeed detectable as a very low energy radiation with a blackbody temperature of 3K.

The discovery of dark matter coupled with the confirmation of the Big Bang Theory necessitated a theory of dark matter that would successfully explain the observable Universe.

In the 1980s, competing theories of hot and cold dark matter (Davis et al., 1985) were proposed. Eventually the cold dark matter theories won out as their prediction of the anisotropies in the CMB (Peebles, 1982) were successfully verified by the Cosmic Background Explorer (COBE) probe (Smoot et al., 1992) in combination with other data sets.

Before the turn of the century, the remarkable discovery of the accelerating universe (Riess et al., 1998) resulted in the resurrection of Einstein's cosmological constant and effectively confirmed ΛCDM as the clear winner among the cold dark matter models. The Big Bang Theory, together with the ΛCDM model, forms much of the basis of modern cosmology and the foundations for theories of galaxy formation and evolution.

0.2 Galaxy Formation and Evolution

0.2.1 Structure Formation in the Universe

The current model of cosmology suggests that there was a single event, the so-called "Big Bang" which resulted in the appearance of expanding space-time containing radiation, followed by an exponential expansion of space known as cosmic inflation (Guth, 1981) which established the initial properties of the Universe as being homogeneous, isotropic and flat. Tiny perturbations in this early Universe are responsible for structure formation. Cosmic inflation also explains the fact that these tiny quantum fluctuations grow into slight ripples of over-density and under-density thus seeding the early stages of structure formation in the Universe.

From a predominantly radiation-dominated Universe, with expansion, the density of radiation drops steeply leading to a the matter-radiation equality at 50,000 years after the Big Bang. Since dark matter only interacts gravitationally, the dark matter ripples from the

fluctuations form compact structures more freely as they are not opposed by other forces such as radiation pressure.

About 380,000 years after the Big Bang, the expansion of the Universe resulted in a lowering of density as well as a cooling down of its temperature to a point where protons and electrons in this plasma soup start combining to form the neutral hydrogen. Electrons decouple from the photons (these decoupled photons are what we detect as the CMB today) and the baryonic matter is now free to collapse under gravity creating local over-densities.

As fluctuations continue to grow, ever larger scales enter the non-linear regime of structure formation where dense concentrations of matter (dark and baryonic alike) get progressively denser. Dark matter begins to collapse into structures known as halos, and baryons fall with the dark matter into these halos. These structures arrange themselves into gravitationally stable configurations, a process known as virialization. The result of this process gives rise to a Universe that resembles a web (the cosmic web) with sheets and filaments of dark matter, creating a skeletal backbone in which star formation and galaxy formation eventually occur.

Within the dark matter halos baryonic matter can, when it becomes dense enough, additionally lose energy by radiation and can sink further into regions of high over-density. The stars and galaxies have their origins in these structures and are the resulting of the cooling of baryons deep in the potential wells of dark matter halos.

While a short summary of how galaxies form would be that the collapse of baryonic matter within dark matter halos results in disk-like structures that then collapse on small scales to form stars, the mechanisms by which this happens is still a topic of debate among astrophysicists. While a top-down scenario, wherein disk galaxies were formed from the collapse

of a single large cloud of gas (Eggen et al., 1962), captures some stages of galaxy formation well, in fact both theory and observations suggest that galaxies grow hierarchically — small galaxies form and merge into larger ones — which complexifies the picture. Meanwhile, the overall efficiency with which baryons form stars depends strongly on the halo mass (e.g. Behroozi et al. 2010), peaking at masses similar to that of the Milky Way. As Somerville & Davé (2015) describe, this dependence probably arises from processes that suppress star formation at lower masses (perhaps due to supernova feedback) and at higher masses (perhaps due to feedback from accreting supermassive black holes).

Since we are limited in our observations by the fact that we cannot observe galaxies in a time-resolved fashion (the time scales are too long), theories regarding galaxy formation rely computational simulations that evolve the initial conditions to the present day. We can compare the galaxies at each epoch to the populations observed at different redshift, assuming large scale homogeneity. As Somerville & Davé (2015) describe, these simulations incorporate the physics of ΛCDM, magnetohydrodynamics, and gravitation. Additionally, these models need to account for a variety of processes on subresolution scales that involve star formation, stellar and AGN feedback, and gas cooling to be able to correctly predict the observed Universe.

Thus, there are still many questions to be answered including and not limited to: how and where the baryons collapse, how galactic disks stabilize, the drivers and mechanisms of galactic feedback and what ultimately causes the relative frequency of different galaxy types in the observable Universe. There are thus many holes in this narrative of galaxy formation and evolution and astronomers are working to bridge this gap in two main ways: from the observational side, this involves accurate measurements of galaxy properties across cosmic

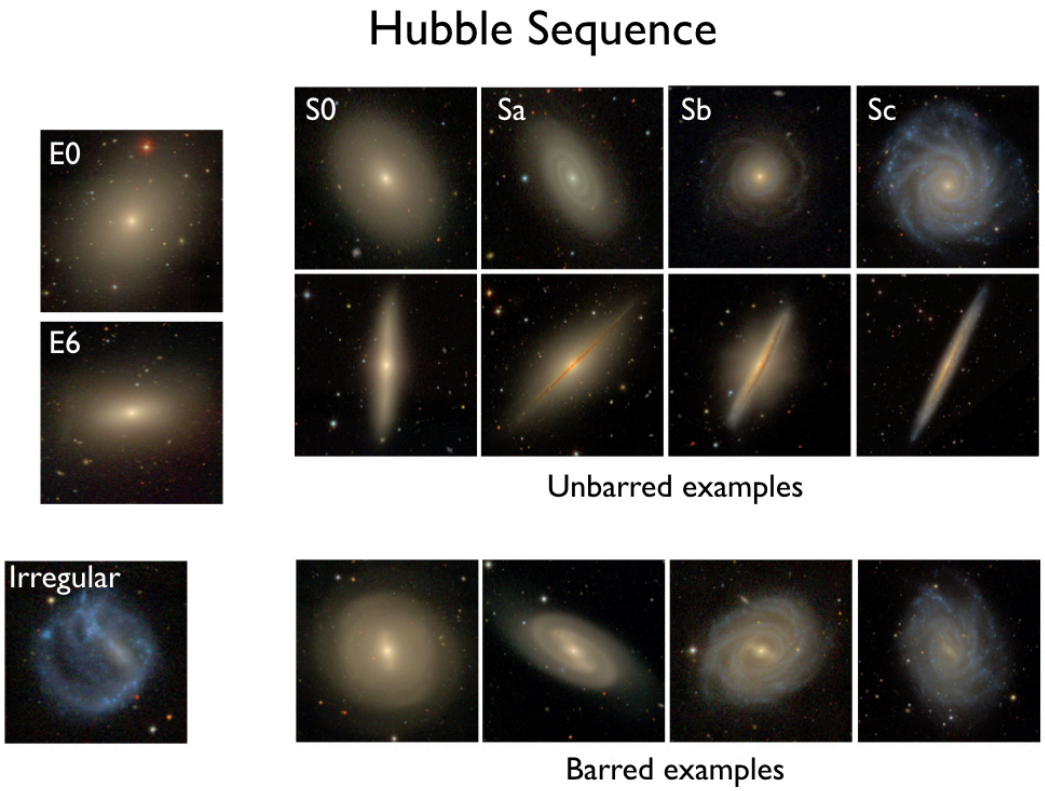

Figure 1: The Hubble Sequence: A classification scheme for galaxy morphologies (Photo credit: ?)

time and from the (theoretical) side of computational astrophysics, this involves fine-tuning the sub-grid models of galaxy formation and evolution simulations so as to be able to reproduce the estimated from the properties. These both take from and in turn inform the parameters in the ΛCDM model of the Universe that cosmologists are engaged in refining.

0.2.2 Galaxy Properties in the Observable Universe

The commonly used classification scheme for galaxies based on their most obvious attribute, the morphologies of their luminous components, was invented by Edwin Hubble in 1926. The classification scheme is based on the relative sizes and of the bulges and disks in galaxies and broadly encompasses four types of morphologies: elliptical, lenticular, spiral and irregular (Fig. 1). Galaxy morphologies are strongly correlated with their other physical properties such as luminosity, age, chemical composition, star formation histories and kinematics (Roberts & Haynes 1994). The bulges usually contain older, redder stars and the disks are characterized by mixed stellar populations along with gas and dust. The disks may also contain spiral arms which usually contain pockets of star formation activity. Elliptical galaxies have almost no disk. Lenticulars are smooth like ellipticals but contain a puffy, thick disk that when observed obliquely has a distinct oval-like appearance (lentil-shaped!). Spirals can have a bulge but are characterized by their thin disk, often with spiral arms. Irregulars are akin to spirals but as their name suggests, appear less organized in their light distribution. Early ideas about galaxy evolution suggested that galaxies formed as ellipticals or lenticulars (referred to as 'early-type' galaxies) and later evolved into spirals or irregulars (referred to as 'late-type' galaxies) and while there are strong correlations between galactic structure and their star formation rates, it is now known that this is in general untrue.

The total amount of light we observe emanating from a galaxy is the second obvious trait that lends itself to comparison. This can be quantified as "luminosity," the amount of energy emitted by a star per unit time, often measured in units of the solar luminosity $L_{\odot}$, and usually measured in a particular wavelength bandpass. Optical or near-infrared luminosity can serve as a reasonable (but not exact) proxy for stellar mass; ultraviolet luminosity can serve as a reasonable (but not exact) proxy for current star formation activity. Observations reveal that fainter galaxies are more frequent per unit volume than galaxies as bright as our own. Very bright big ellipticals are much rarer than both. The distribution of galaxy luminosites, per volume and per unit luminosity, is known as the "luminosity function" (Blanton et al. (2005); Efstathiou et al. (1988)), which provides key constraints on galaxy formation and evolution.

The total luminosity of a galaxy in the ultraviolet through near infrared is generally dominated by stars, and the stellar population is changing with time as stars evolve off the main sequence and reach their fates, for example as black holes, neutron stars, or white dwarfs. A more stable and sometimes more interesting quantity is the total mass in stars, the stellar mass. Because the luminosities of stars varies as $L \propto M^{-\alpha}$, where $\alpha \sim 3$–5, and the more massive stars die rapidly, the total ratio of luminosity to stellar mass varies over time. Furthermore, because the massive stars are very hot, the overall color of the stellar population starts out blue and becomes increasing red. This pattern leads to a relationship between the galaxy spectrum and the stellar mass to light ratio, that can be exploited to estimate the stellar mass of a galaxy.

The most basic measure of the spectral energy distribution of galaxies are its colors. Colors in astronomy are defined on the basis of the ratios of observed fluxes in various band-

passes. For instance, $g - r$ is $2.5 \log_{10}$ of the ratio of the r-band to g-band flux, where g and r are optical bandpasses used in the Sloan Digital Sky Survey (SDSS); larger $g - r$ indicates a redder galaxy. Galaxy populations have a bimodal distribution and can be divided into the so-called "red sequence" and "blue cloud" (Blanton et al. (2003); Strateva et al. (2001)). The blue cloud is dominated by star-forming blue spirals with young stellar populations; the red sequence has a mixture of varied populations, including some older or dust-reddened spirals, lenticular galaxies, and ellipticals. The intermediate colored population, the so-called "green valley", must contain (but does not only contain) the population of galaxies that are in the process of ending their star formation and transitioning from blue to red. However, a complication to this simple interpretation of the observations is the presence of dust, which has the tendency to make galaxies appear redder. We investigate the star formation of galaxies in the context of optical colors and dust, further in Chapter 1.

The last significant observable property we introduce here is the galaxy environment, which is a measure for each galaxy of how many other galaxies are nearby it relative to the mean galaxy density. Galaxies exhibit substantial clustering relative to a Poisson distribution, leading to a large dynamic range in local density For example, a galaxy like the Milky Way most commonly has not similarly massive neighbors within 1 Mpc, but massive clusters of galaxies have 100s of Milky Way-sized galaxies within a Mpc. This clustering of galaxies reveals information about cosmological parameters, like the initial amplitude of fluctuations and the mean dark matter density.

The environment of galaxies also appears to be correlated with their formation history, as manifested by their morphology (Dressler, 1980), luminosity (Norberg et al., 2002), star formation rates (Lewis et al., 2002), and numerous other properties. For instance, simplis-

tically, blue galaxies preferentially exist in isolated environments (or voids) and large red ellipticals preferentially exist in clusters. Galaxy environments can be measured in a variety of ways, such as counts in a projected aperture or distance to nearest neighbor (Cooper et al., 2005). The density field length scales at which galaxy environment matters significantly enough to affect its star formation has been investigated; it appears that the local environment (within 1–2 Mpc) is most important, with the larger scale environment being of much less importance at a fixed local environment (Blanton et al. (2006); Kauffmann et al. (2004); Park et al. (2007)).

0.2.3 Questions in Galaxy Evolution

The lifecycle of a galaxy can be thought of in terms of the timeline of the events between the formation of the first stars in the galaxy began to when there is little to no star formation activity in the galaxy, i.e. the galaxy is quenched. Many processes determine the history of star formation and how it may end. Star formation begins with the inflow of gas, its formation into galactic disk structures, its radiatively cooling, the formation of molecular clouds, and the formation of stars. The stars form in some initial mass distribution whose form in the Milky Way is constrained observationally, but whose variation among galaxies is largely unknown. The massive stars in the stellar mass distribution tend to disassociate and ionize the surrounding gas, dispersing the cloud that is forming stars. This feedback can even heat or remove surrounding gas clouds in the disk. Other feedback processes, such as accreting supermassive black holes at the centers of galaxies, can also remove gas and suppress star formation. For most massive galaxies, including the Milky Way, current star formation rates are rapid enough to consume the remaining gas in 2–3 billion years; this fact is

widely interpreted to indicate that to remain star forming, galaxies require a steady inflow of gas from the external environment.

Models of galaxy formation built from numerical hydrodynamic simulations (Crain et al. (2015); Davé et al. (2016); Sijacki et al. (2015)) are powerful enough now to predict this evolutionary process in a cosmological context. However, they can typically resolve scale of only 100 pc or so, which is far larger than a forming star or even an individual massive molecular cloud. The detailed star formation and feedback processes are therefore the product of subgrid physics (Agertz et al., 2007) that are calibrated on the observations themselves. There are a number of free parameters in the subgrid models, characterizing the rate of star formation as a function of local conditions, the effects of supernova (Creasey et al., 2013) and stellar feedback (Hopkins et al., 2012), the activity of supermassive black holes, and other effects. The calibration of the parameters used for these simulations, and the use of the simulations as a test of the overall picture for cosmological galaxy formation, therefore requires that the observations they are calibrated on and compared to are correct.

The stellar mass and star formation rates of galaxies represent a coupled pair of galaxy properties that are critical in this process. The stellar mass function (analogous to the luminosity function) has a shape very different than the halo mass function, with a shallow slope at the faint end and a steep cutoff at the bright end. This shape implies that star formation is suppressed at the highest masses, and also at low masses. The simulations generally explain these features using supermassive black hole feedback at high mass and supernova feedback at low mass. The degree and type of feedback required is determined by the observed stellar mass function.

The star formation patterns are also informative. For star-forming galaxies, the star for-

mation rates scale approximately as $\dot{\mathcal{M}}_*^{2/3}$ (Noeske et al., 2007). Fully quenched galaxies are found at the highest masses and/or in the densest regions. What determines the star formation rates, and what processes quench some galaxies, are important questions the simulations are designed to help answer. The simulation parameters can be tuned to produce these patterns, but the meaningfulness of those tuning parameters, and the legitimacy of additional predictions the simulations may make, depends on the reliability of the observations they are tuned to.

0.3 Observational Indicators of Star Formation and Stellar Mass

In this section we will review how astronomers observationally infer star formation rates and stellar masses in galaxies.

0.3.1 Integrated Star Formation Rates for Galaxies

Since we know that star formation ultimately is the result of the collapse within Giant Molecular Clouds (GMC) of cold gas, it follows that the star formation rate in a galaxy must relate to the availability of cold molecular gas. It was first proposed by Schmidt in 1959 (Schmidt, 1959) that star formation in a galaxy scales with the the surface density of gas in the galaxy. As reviewed by Kennicutt (1998), the mean surface density of galaxy star formation rate is approximately related to the mean surface density of the cold gas in the galaxy (neutral plus molecular gas) by a power law known as the Kennicutt-Schmidt Law:

$$\mathrm{E}_{\mathrm{SF}} = A\mathrm{E}_{\mathrm{g}}{}^{N}$$

The determination of N relies on a host of empirical studies based on gas content and star

formation from a host of disk and starburst galaxies and is found to be $\sim 1.3 - 1.5$. The neutral gas content is detected through emission from the 21 cm hyperfine transition of hydrogen, assuming a cosmic mean helium fraction. Molecular gas is dominated by H_2, which unfortunately does not have strong emission lines at typical molecular cloud temperatures. The molecular gas mass is typically inferred from trace molecules like CO and HCN.

To be able to infer star formation rates from galaxies, one has to investigate their stellar populations. As it is almost impossible to resolve stars in galaxies (barring the closest ones) even with space telescopes, to get the star formation properties of a galaxy, we rely on integrated light measurements in the Ultraviolet (UV) and Infrared (IR) continuum or the so-called nebular recombination lines. A comprehensive review of this subject can be found in Kennicutt & Evans (2012). For instance, because short-lived, massive stars have high temperatures at their surface, the continuum luminosity integrated across the blue or near-UV part of the spectrum is an indicator of recent star formation. The quantitative relationship between recent star formation and the UV light depends for its calibration on evolutionary synthesis models (Section 0.3.2) and an assumption about the stellar initial mass function (IMF), since the bulk of the stellar mass is in low mass stars, but the bulk of the light comes from the massive stars. For example, Madau et al. (1998) and Kennicutt & Evans (2012) report calibrations (assuming a Salpeter IMF; Salpeter 1955): relative to the UV Luminosity L (in a wavelength range of 1500?2800 Å):

$$\mathrm{SFR}\ (\mathrm{M_\odot yr^{-1}}) = 1.4 \times 10^{-28} \mathrm{L} \quad (\mathrm{ergs\ s^{-1}})\ \mathrm{Hz^{-1}})$$

A significant issue with inferring a UV star formation rate is the presence of dust in galaxies. Dust absorbs a significant fraction of the bluer part of the spectrum, and because

of its low temperature re-emits the absorbed energy in the mid- and far-infrared. Any UV star formation measurement thus needs to account for this dust attenuation. Furthermore, because of these effects, the infrared light (10–100 μm) is a tracer of the star formation rate as well. we will discuss further these issues further in Chapter 1.

Star formation in galaxies, specifically the production of hot and massive stars, results in the heating and ionization of gas in the Interstellar Medium (ISM), which in turn leads to observable line emission. The most significant of these are the Balmer emission lines due to emission from Hydrogen during the recombination processes that balance the ionization processes in the nebulae surrounding hot stars. These nebulae are known as HII regions, and the presence of HII regions in a galaxy and their characteristic Balmer line emission is thus a probe of a young massive stellar population. The strongest of these recombination lines in the optical is the $n = 3$ to $n = 2$ transition, the $H\alpha$ line at 656.28nm. During the recombination process, electrons enter at typically high n states. following that event, any direct transition from some high n to the $n = 1$ state will lead to a photon which is quickly absorbed under nebular conditions by exciting another nearby atom. This resonant scattering continues under the photon is absorbed on dust, or a rare 2-photon decay occurs from the $2s$ state, or Doppler shifts scatter the photon into the wings of the absorption line. The net effect is that almost every ionizing photon leads to a Balmer photon. The ratio of the resulting Balmer lines to each other can be calculated and is relatively constant, with weak dependence on temperature or electron density. Thus, one of the most widely used estimators of SFR is a linear function of the emission line luminosity of the $H\alpha$ line (Kennicutt

et al. (1994); Madau et al. (1998)):

$$\mathrm{SFR}\ (\mathrm{M}_{\odot}\mathrm{yr}^{-1}) = 7.9 \times 10^{42} \mathrm{L}(\mathrm{H}\alpha)\ (\mathrm{ergs\ s}^{-1})$$

The bluer Balmer emission lines such sa as $H\beta$ are intrinsically weaker, and often substantially dust-reddened.

Collisionally excited lines such as the [OII] doublet at 3727 Å also correlate with star formation, but are much more sensitive to the metallicity, temperature, and density of the gas.

All the star formation rates discussed above assume some priors on the evolution of the galaxy from the IMF chosen to the timelines of starbursts and effective stellar population synthesis models are required to be able to successfully account for the spectral energy distribution of the galaxy and give accurate insights into the stellar and dust content of the galaxy.

0.3.2 Spectral Diagnostics and Stellar Population Synthesis Models

The galaxy spectrum contains an imprint of its Star Formation History (SFH), stellar metallicity and abundance pattern, stellar Initial Mass Function (IMF), total stellar mass and the nature of its gas and dust content. However, to be able to interpret the details in a spectrum accurately, one has to rely on evolutionary synthesis models or what are called Stellar Population Synthesis (SPS) models. Typically these models contain a comprehensive library of stellar spectra of stars across ages, masses and luminosities. The earliest such models (Spinrad & Taylor 1971; ?) relied on using a linear combination of the diverse individual stellar spectra to reconstruct the integrated light emission from a galaxy. However, popu-

lations of stars do not come in arbitrary mixes — stars are formed together in groups that evolve over time in a regular way. More recent models (Bruzual & Charlot 2003a; Leitherer & Heckman 1995; ?) involve setting handful of global parameters, such as the IMF, the SFR, the rate of chemical enrichment, and using the laws of stellar evolution and of stellar atmospheres to predict the emergent integrated spectrum of the population as it evolves in time.

Broadly speaking, SPS models require the following ingredients (?): an IMF, stellar evolutionary tracks (isochrones), stellar spectral libraries, and a SFR and chemical evolution model. The choice of IMF (Chabrier 2003; Kroupa 2001; Salpeter 1955) determines the distribution of stellar masses initially and the spectral libraries convert the stellar evolution outputs such as surface gravity and effective temperature into observable Spectral Energy Distributions (SEDs). The spectral libraries can either be calculated theoretically (??) or on a purely empirical basis and are oftentimes a combination of both. Some notable modern stellar spectral libraries constructed from observations are ELODIE (Prugniel & Soubiran, 2004), STELIB (?), MILES (Sánchez-Blázquez et al., 2006), and most recently MaStar (Yan et al., 2018).

The next step in reconstructing the SED of a galaxy is to account for the effect of the Interstellar Medium (ISM) on the integrated light from the simple stellar population. The ISM primarily consists of gas and dust, and a model to account for the radiative transfer through the ISM is needed. Photoionization codes such as CLOUDY (Ferland et al., 2013) account for the ionization of atomic gas by star light. The more significant effect on the SED comes from dust which redistributes the flux densities via scattering and absorption from the bluer part of the spectrum, re-emitting absorbed light in the infrared. Models of

dust (Calzetti et al. 2007; Draine & Li 2007) are thus almost always combined with the SPS models.

The evolutionary synthesis models combined with the dust models can effectively predict galaxy SEDs at any instant in its cosmic history as needed, thus enabling them to be able to be compared to photometric or spectroscopic data from galaxies at arbitrary redshifts. The method of fitting observed data using a SPS model to infer the physical properties of a galaxy is known as SED fitting. The input data can either be in the form of photometric broadband fluxes or observed spectra and sometimes, spectral indices. A recent review on the subject of SED fitting can be found in Conroy (2013).

SED fitting requires searching a large model space of the SPS and dust libraries and evaluating how well-matched to observations are the predicted SEDs for a chosen set of parameters relating to the SFH and dust attenuation. SED fitting codes employ a range of techniques, to perform this mimization; examples of these codes are MAGPHYS (da Cunha et al., 2008), CIGALE (?) and Prospector (Leja et al., 2017).

There are a couple of things worth noting about SED fitting. Firstly, all the parameters except for the overall normalization are set by the "shape" of the spectrum, i.e., the observation flux ratios between photometric bandpasses ("colors") or spectral channels. Thus, parameters like the dust attenuation, metallicity, age of the stellar population, are independent of the bolometric luminosity. It is often convenient to derive parameters like the mass-to-light ratio (M/L) of the galaxy, the Specific Star Formation Rate (SSFR, the SFR per unit solar mass), dust attenuation, and metallicity. Secondly, the robustness of fitting an SED to observed spectrometric and photometric data relies a lot on how the systematic uncertainties in the SPS (and dust) models are accounted for. Thus the priors on the SFH

and dust libraries can significantly impact the inference of the stellar mass, SFR and mean stellar age.

0.3.3 Inferring $\mathcal{M}_*$ and SFR from SED fitting

While historically the way galaxy masses have been estimated is by looking at rotation curves and the kinematics within a galaxy, for galaxies apart from the closest ones this information is often unavailable. Thus, similar to what we have discussed with regards to SFR indicators in Section 0.3.1, we have to figure out a way to meaningfully infer the total stellar mass content ($\mathcal{M}_*$) from a galaxy by looking at its integrated light. One of the main parameters constrained by the SED shape of a galaxy is the Mass-to-Light ratio (M/L) from which the stellar mass can be obtained by multiplying the luminosity within the wavelength range under consideration.

The easiest way to obtain M/L ratios involve using their relationships with color. Bell & de Jong (2001) used the Bruzual & Charlot (2003a) SPS models to map the relationship between M/L and color as a function of metallicity and SFH. (Zibetti et al., 2009) also later developed tables for the color-M/L relationship using a library of model galaxy SED's. A related way to estimate stellar masses is by using SED fitting methods on broadband photometry. Of the physical parameters interpreted via SED fitting, stellar masses tend to be relatively robust (Muzzin et al., 2009; Papovich et al., 2001), especially in comparison to SFR estimates. One reason for this maybe that that the effect of dust-reddening is very minimal on the SFH-metallicity variations in the color-M/L plane. However both these methods are hugely affected by the SFH uncertainties inherent in using SPS models, especially in terms of accounting for the bursty star formation episodes. One way this can be resolved is by

looking at spectroscopic indicators of starburst that are not affected by the age-metallicity degeneracy.

Higher metallicity in the ISM and dust tend to manifest themselves in the spectra of unresolved stellar populations in galaxies in a very similar way to what they would look like if they had older mean stellar ages and this effect is known as the age-metallicity degeneracy Worthey (1994). Kauffmann et al. (2003) used a combination of two spectral indicators (Section 2.2), the H_{δ_A} absorption index (representing the Balmer transition from $n = 2$ to $n = 6$ levels) and the D_n4000 index (which is representative of the 4000 Åbreak found in the spectra of galaxies) to constrain the M/L ratios of galaxies. They did so by using a suite of observed spectra from SDSS and a SPS model to fit for the spectra. While the age-metallicity degeneracy does indeed affect the Balmer lines, the two aforementioned indices together provide a robust M/L constraint. They obtained 95% confidence limits on stellar masses of 0.2 and 0.3 dex and these are part of the most popularly used catalogues, the MPA-JHU SFR and $\mathcal{M}_*$ catalog. I investigate the affects of aperture correction in the MPA-JHU catalog using spatially resolved spectra in Chapter 2.

Surprisingly, the uncertainties in spectroscopically based stellar masses obtained by fitting observed optical spectra (Chen et al., 2012; Kauffmann et al., 2003) are not significantly better than the color-based stellar masses, except for galaxies with unusual SFH's Gallazzi et al. (2005). However, spectroscopically derived masses are more robust to dust attenuation than photometric masses (i.e. stellar masses obtained by fitting broadband photometry). Examples of photometrically derived masses using SPS models can be found in Blanton & Roweis (2007); Drory et al. (2004)

SFR measurements using SED fitting are dependent on the SFH shape (i.e. star forma-

tion as a function of time) used by the evolutionary synthesis models. For instance, typically in the modeling of early-type galaxies, the SFHs are represented as an exponential decay whose half-life is a parameter that is constrained by the SED fitting method used. The choice of priors on the SFH libraries can thus create high systematic uncertainties in SFR and stellar age estimation. The priors on dust modeling and the age-metallicity degeneracy inherent in SEDs can cause further challenges and thus, in the absence of high quality data, SFR estimations from SED fitting cannot be relied upon without fully understanding the nature and extent of these biases.

The aforementioned MPA-JHU catalog contains SFR estimates for SDSS galaxy spectra using the Brinchmann et al. (2004) method of modeling a suite of optical emission lines with model parameters including metallicity, dust attenuation, ionization parameter, etc. Salim et al. (2007a) used broadband photometry instead from a similar sample of SDSS galaxies along with UV photometry from GALEX using SPS models with a range of exponentially declining and bursty SFH's, metallicities and dust attenuation. Their comparison with the MPA-JHU SFR's showed that in general the two SFR's are in good agreement with the offset being the result of differences in optical depth accounted for by dust attenuation. Alternative ways of constructing SFH libraries include using semi-analytical models, the results of hydrodynamic simulations or using non-parametric SFH's. In general, SED-based SFR's, when a fixed IMF is assumed, are consistent within a factor of two level (Conroy, 2013).

The estimations of SFR and $\mathcal{M}_*$ of galaxies rely heavily of the availability and quality of data. Over the last decade, these have improved significantly, thanks to the high quality multi-band photometry as well as spectroscopy, including spatially resolved spectra, that

have been collected by various ground-based and space-based observatories. I review the significant observational surveys related to these observatories along with the major results gleaned from them in the next section.

0.4 Star Formation in the Local Universe

0.4.1 The Age of Digital Survey Astronomy

Redshift surveys in astronomy have their origins in the early 20th century when astronomers were interested in investigating Hubble's Law and the large scale structure of the Universe. The CfA redshift survey (1977) was the first systematic attempt at mapping a section of the sky and was later extended to the CfA2 survey which successfully obtained the spectra of 15,000 galaxies in the 1990s. With the advent of fibre-optic and multi-slit spectrographs which allowed for simultaneous observations of hundreds of galaxies, larger redshift surveys such as the 2dF Galaxy Redshift Survey (2dFGRS) (cite), the Sloan Digital Sky Survey (SDSS) (cite), the Galaxy and Mass Assembly (GAMA) Survey (cite) , etc. have enabled astronomers to be able to study the physical properties of galaxies in a statistically rigorous manner.

The choice of survey or sample of a survey that one uses to build a dataset depends on the particular question in galaxy evolution that is being investigated. Thus, understanding the redshift limits of the survey (the so-called depth of a survey) or subsample that is being used to construct a volume-limited dataset is a crucial step in this process. In this thesis, we only concern ourselves with the local Universe out to redshifts of $z < 1.5$ as the goal is to understand the limitations of some of the most commonly used SFR and $\mathcal{M}_*$ indicators. The angular coverage of a survey is also of importance, especially if environment measures

play a significant role in the analysis. Keeping these in mind, the surveys I have worked with are derived from the SDSS Legacy sample.

The SDSS is the largest multi-spectral and multi-imaging spectroscopic survey thusfar that has been carried out using a 2.5m wide angle optical telescope at the Apache Point Observatory (Gunn et al. 2006) in New Mexico, United States since 2000. (all the citations: York et al. 2000; Strauss et al. 2002, ..?). SDSS covers 14,555 square degrees on the sky (a little over 35% of the sky) up to depths of $z = 0.1$ for the main galaxy sample and out to $z = 7$ for the distant quasars. The Legacy Survey covers the first 8 years of the SDSS run and provides a uniform, well-calibrated map in *u, g, r, i* and z bands of around 8000 square degrees of the sky including the North Galactic Cap and three stripes in the South Galactic Cap.

The NASA-Sloan Atlas (NSA) Catalog is a catalog of images and parameters of local galaxies up to redshifts of $z = 0.055$ that is derived from SDSS imaging, with additional UV broadband photometry from the space-based Galaxy Evolution Explorer (GALEX). The NSA is built from a reanalysis (cite Blanton et. al. 2011) with of the SDSS Legacy photometry, with better object detection and deblending, making it better tuned for large, bright galaxies than the typical SDSS processing. This makes the NSA the ideal candidate to study the physical properties of galaxies in the Local Universe and I use the NSA to compare two star formation indicators in the context of dust in Chapter 1.

Apart from broadband photometry, SDSS also uses a multi-slit spectrograph (cite Abazajian et al. 2009) to obtain the optical spectra of targeted galaxies. The spectra are taken using 3 arcsec diameter fibres and have a wavelength range of 3800-9200 Å. Some of the major results in galaxy formation and evolution have been possible because of the SDSS spectroscopic survey (Section 0.4.2). However, the major limitation of spectroscopic surveys has

been that due to the limited size of the fiber, only a small sub-region of the galaxy defined by the size of the fiber and the orientation of the slit ends up being sampled, thus not giving us enough insight into the internal structure and dynamics of the galaxy. Additionally, one has to adequately fibre-correct any measurements made using the spectra. This has thus engendered the field of integral field spectroscopic surveys such as MUSE, SAMI, MaNGA, etc which aim to obtain spatially resolved spectra for significantly large samples of galaxies in the local Universe. Mapping Nearby Galaxies at Apache Point Observatory (MaNGA), is the largest such survey of that nature undertaken so far with a view to observe 10,000 galaxies by 2020 across a wide dynamic range in M_*, environment, and SFR with uniform radial coverage. The target selection for MaNGA is based on the NSA and so far, close to 6000 galaxies have been observed via MaNGA. I use this sample of galaxies to analyze the robustness of the aperture corrections made by cite Kauffmann by looking at the galaxies through multiple apertures and comparing the observed M/L ratios obtained thus in Chapter 2.

0.4.2 Major Results from SDSS: Stand-in Title

0.4.3 This Thesis

Brief overview of structure of thesis

1

UV to IR Star Formation Indicators and Environments

1.1 Introduction

Determining the formation history of galaxies is one of the most important tasks in astronomy. The average star formation rates of galaxies have reduced with cosmic time (as reviewed by Madau & Dickinson 2014) and star-forming galaxies "transition" to red and quiescent ones over that time (*e.g.* Ilbert et al., 2013; Moustakas et al., 2013; Muzzin et al., 2013; Peng et al., 2010; Tomczak et al., 2014, among others). Many mechanisms have been proposed to explain the observed patterns of galaxy evolution but there are many unresolved questions regarding them. These mechanisms are known to have a some correlation with the environment, due to the fact that galaxy type depends on environment in the present day (Blanton & Moustakas, 2009a; Dressler, 1980).

Star formation rate estimates are an important tool in the observational study of this problem (Kennicutt & Evans, 2012). The light emitted from galaxies can reveal recent star formation through the ultraviolet light of massive stars, recombination line emission in the ionized gas around those stars, in infrared light from dust in the galaxies absorbing the ultraviolet starlight, and from radio synchrotron emission from the ionized gas. Ultraviolet, optical, and infrared images and spectra are available for numerous low redshift galaxies, from the Sloan Digital Sky Survey (SDSS; ?), the Wide-field Infrared Survey Explorer (WISE; Wright et al. 2010), and the Galaxy Evolution Explorer (GALEX; ?).

In this chapter we compare two specific ways to estimate star formation rates from imaging photometry. We concentrate on imaging because it usually provides the most complete census of the galaxy; spectroscopy is often of only part of the galaxy, usually the center. We are interested specifically in comparing ultraviolet-based star formation indicators with

indicators that account for the infrared light. The main difference between these types of indicators is how they account for dust absorption. The former ostensibly are corrected for dust absorption, but we generally expect that the latter should be more reliable and complete. However, detectable infrared light is not always available.

The presence of dust is an important complication in any analysis of galaxy light. Dust absorbs preferentially in the UV/optical region of the galaxy spectrum and both extincts and reddens the photometric data. The extinction in the visual bandpasses in star forming galaxies is highly variable but is commonly of order 50%. This energy is re-emitted in the mid- to far-IR by poly-cyclic aromatic hydrocarbon molecules as well as warm and cold dust grains. Recent studies (Burgarella et al. 2013) find that in the nearby universe, almost 70% of the FUV luminosity is obscured by dust on an average. Although UV estimates of star formation do attempt to account for dust attenuation (Salim et al. (2007b)), the extensive reliance on UV SFR in the literature (*e.g.* Karim et al., 2011; Lee et al., 2009; Moustakas et al., 2013; Peng et al., 2010; Wyder et al., 2007, among others) makes it important to understand how well the dust corrections for UV SFR estimates work relative to other methods of estimating SFR.

Here, we examine a sample of galaxies whose UV-IR photometry is available and estimate the star formation rate in two independent ways. First we exploit the fact that we have UV to IR photometry and perform SED fitting using MAGPHYS (da Cunha et al., 2008), which accounts for dust by using a simple method of energy balance to obtain the specific star formation rates (SSFRs). The other method involves using purely UV photometry to estimate both star formation rate and dust attenuation using the prescription given by Salim et al (Salim et al., 2007b). We also estimate the environments of our population.

We ask the following questions of this sample. How do these different star formation estimators disagree with each other? How does each estimate correlate with environment? Does one trace environment more closely? Under the assumption that the environment primarily correlates with the SSFR rather than dust obscuration's effect on the observables, studying this correlation will yield insights into the relative accuracy of the methods.

1.2 Constructing a local sample spanning Ultraviolet to Infrared Imaging

The sample on which we perform our measurements is based on the NASA-Sloan Atlas, a nearby galaxy sample which includes optical and ultraviolet imaging from SDSS and GALEX. We use NSA version `v0_1_2`, whose redshift range extends up to $z = 0.055$ and includes SDSS (Data Release 9) and GALEX imaging for galaxies. The total number of objects in this NSA catalog is $\sim$150, 000. We define two samples from the NSA, one that we use to define environment (Environment Determining Population or EDP, hereafter) and one for which we determine star formation rates (Star Formation Rate Population or SFRP hereafter). We note that the SFRP is a subsample of the EDP. To get our EDP, we impose a volume-limited cut on this sample by retaining only galaxies with $-24.5 < \mathcal{M}_r < -18.5$, which leaves us with 95, 638 galaxies.

The star formation rate determinations we use here require both UV data and IR data. About 80% of our galaxies have UV data from GALEX analyzed in the NSA. To obtain infrared imaging for the data we use the Wide-Field Infrared Survey Explorer (WISE) data and match the objects from the NSA with the ALLWISE Source Catalog to get the four-band infrared fluxes for each galaxy. About 99% of galaxies in this sample have WISE data. We intend to study the evolution of these galaxies through the optical-IR color space, and

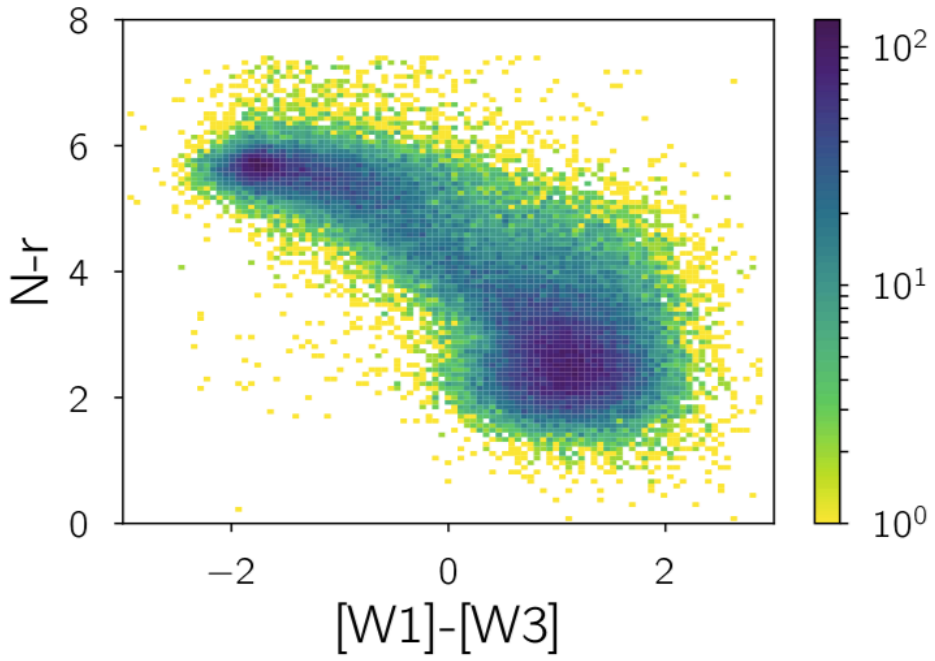

Figure 1.1: The local sample distribution across optical and IR colors

therefore remove all galaxies with missing/faulty photometry in GALEX, SDSS, or WISE. This process includes limiting the color range of objects in the optical ($7.5 > N - r >= 0$) and infrared ($3.0 > [W1] - [W3] >= -3.0$) colors (top left corner of Fig. 1). In addition, we remove some objects near the edges of the sample, which do not have reliable environment determinations (see Section 1.4.2). Our SFRP ultimately consists of 61, 046 objects with absolute magnitudes in the UV (F and N bands), optical (u, g, r, i and z bands) and infrared ($W1$, $W2$, $W3$ and $W4$ bands).

1.3 Estimating the Specific Star Formation Rates

We compare two approaches to calculating specific star formation rates (SSFRs). The first uses UV, optical, and IR data. The second uses only the UV data.

1.3.1 SED Fitting - MAGPHYS

We develop here a method to quickly estimate SSFRs based on UV-optical and infrared colors. We begin by sorting galaxies into bins of the $(N-r)$ - $([W1]-[W3])$ color space (25×25 bins, where the optical and IR bin sizes are 0.29 and 0.24 in magnitudes respectively). Within each bin, we normalize the fluxes of each galaxy relative to a constant flux in the r-band, and then take the mean normalized flux in each band over all galaxies in the bin. This procedure yields a "template" SED for each bin in the color-color space.

We then use Multi-wavelength Analysis of Galaxy Physical Properties (da Cunha et al. (2008)) software to infer the SSFR for each template SED. MAGPHYS is a physical model-based method to interpret the mid- and far-infrared spectral energy distributions of galaxies, self-consistently modeling the emission at ultraviolet, optical, and near-infrared wave-

lengths. For every input galaxy with a set of observed fluxes in different bands, MAGPHYS generates an optical and infrared library at that redshift and then samples all template spectra whose fluxes obey a simple principle of energy balance: that the amount of energy absorbed by dust in the UV/Optical matches the amount of infrared emission that is accounted for purely by dust. Once the templates have been sub-sampled thus, MAGPHYS uses chi-squared fitting to see which combination best reproduces the observed fluxes along with the likelihood for the distributions. The results for the SSFRs thus obtained for each template are shown in the lower left panel of Fig 1.2 along with the number distribution of the galaxies across the chosen bins. Note that bins with < 5 galaxies were omitted as those regions of the color-color space are obviously under-sampled.

The resulting distribution of the MAGPHYS-based SSFRs across the color-color space looks as we would expect it to for the most part. In UV-optical colors, blue galaxies have high SSFRs, and red galaxies have low SSFRs. However, there is also a dependence of SSFR on IR color; most notably, in the UV-optical green valley, the redder galaxies in the IR have higher SSFRs. These galaxies are likely to be dust-extincted in the UV, with the reemission by dust reddening the IR colors. In what follows, we will use the UV-optical and IR colors of individual galaxies, and the dependence of the SSFR on these colors shown in the lower left panel of Fig 1.2, to assign an SSFR to each individual galaxy.

1.3.2 UV Star Formation Rates

We also explore a simple method of determining star formation rates developed by Salim et al. (2007b) that depends only on the UV fluxes of each galaxy. It assigns a star formation rate that is proportional to the UV luminosity (specifically the FUV band if we are looking

at GALEX). Dust attenuation is also accounted for in this method by looking at the ratio of luminosities in the FUV and NUV bands.

According to this prescription (Salim et al., 2007b), the star formation rate is given by:

$$SFR = 1.08 \times 10^{-28} L^{\circ}_{\rm FUV},$$

where L°_{FUV} is the rest-frame FUV luminosity. This method accounts for dust attenuation of the FUV light as well by estimating an attenuation factor Av as follows.

If $N - r \geq 4.0$, i.e. for the red sequence galaxies,

$$Av = \begin{cases} 3.32(F - N) + 0.22, & \text{if}(F - N) < 0.95 \\ 3.37, & \text{if}(F - N) \geq 0.95. \end{cases}$$

If $N - r < 4.0$, i.e. for the blue sequence galaxies,

$$Av = \begin{cases} 2.99(F - N) + 0.27, & \text{if}(F - N) < 0.90 \\ 2.96, & \text{if}(F - N) \geq 0.90. \end{cases}$$

This method uses the UV slope to estimate the dust attenuation. The physical idea is that when the UV light is dominated by massive young stars, these are hot enough that we are observing their Rayleigh-Jeans tail spectra, and this slope is basically constant with age of the population. Thus the observed UV color reveals the dust reddening.

The lower right panel of Fig. 1.2 shows the mean $\rm SSFR_{UV}$ as a function of color. Compared to the lower left panel, the $\rm SSFR_{UV}$'s have a nearly monotonic relationship with UV-optical color whereas, as discussed above, the $\rm SSFR_{MAGPHYS}$'s do not. Assuming the $\rm SSFR_{MAGPHYS}$'s

are closer to correct, the UV-optical green valley contains a population of galaxies that are not truly transitioning but instead are reddened by the presence of dust. Furthermore, the nominally dust-corrected UV star formation rates do not successfully identify these galaxies.

MRB: Quantify the fraction of galaxies like this; say within $2.5 < N - r < 4.5$, what fraction have $[W1] - [W3] > 1.5$, answering same question in 3 bins of absolute magnitude too.

1.4 Environments

We identified above a population of galaxies isolated in color space, which appeared to have dust-extincted star formation, such that the $\mathrm{SSFR}_{\mathrm{UV}}$ estimate was much less than the $\mathrm{SSFR}_{\mathrm{MAGPHYS}}$. In order to confirm whether MAGPHYS is capturing an inherent property in this population of galaxies, we examine an independent physical property, namely the environments of our sample.

1.4.1 Measures of Environment

The environment of a galaxy can be defined in many ways, such as fixed aperture counts, distance to the n^{th} nearest neighbor, Voronoi volumes, etc (Cooper et al., 2005). Here we use counts in a projected fixed aperture of radius 0.5 Mpc as our environment measure. Around every galaxy we construct a projected cylinder with a radius (in the transverse direction) of $r_t = 0.5$ Mpc and a line of sight velocity window of $v_{los} = \pm 1000 km/s$. For each galaxy for which we have star formation measurements, we count its number of neighbors (n_{env}) in this cylinder(Fig. 1.2) in the Environment Defining Population.

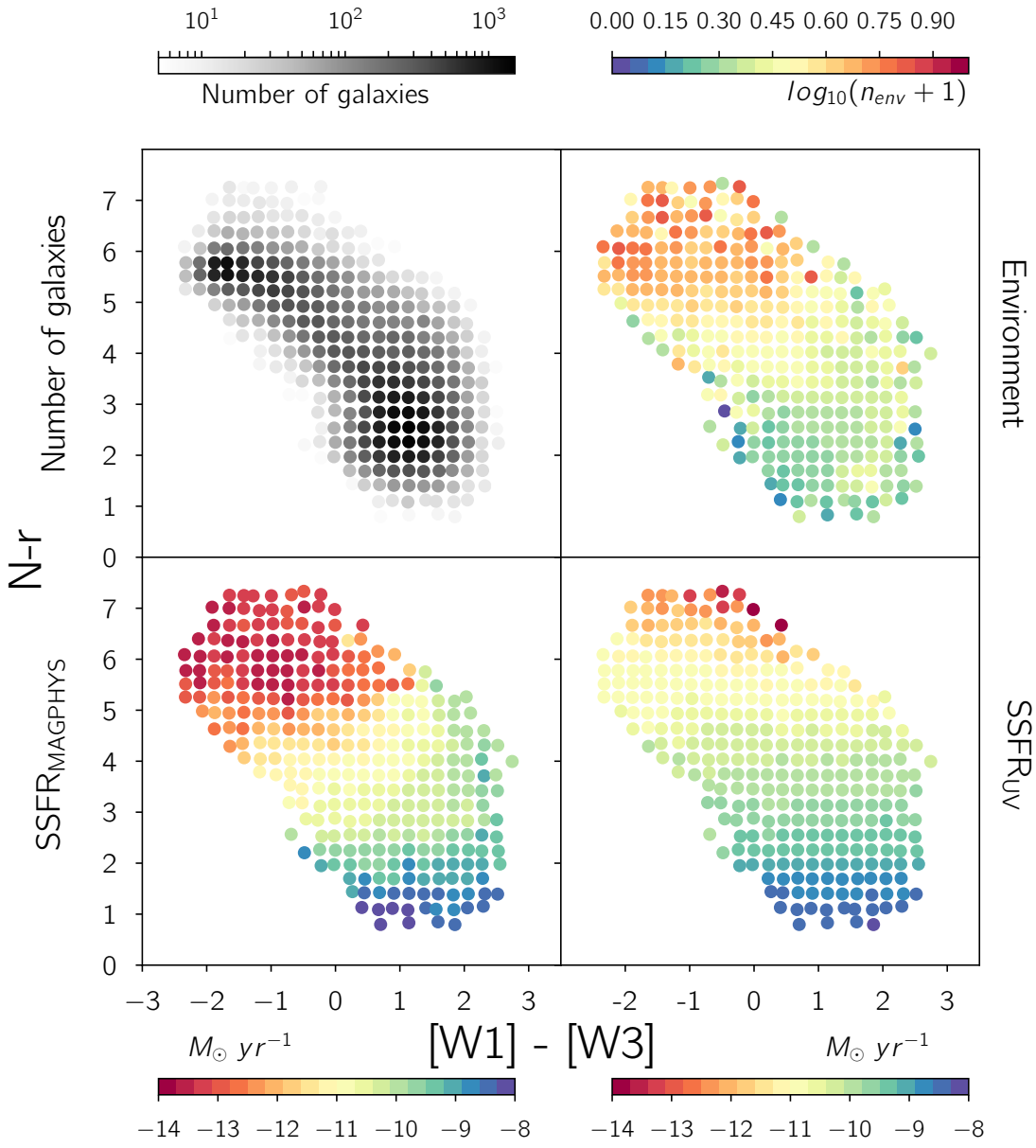

Figure 1.2: The SSFR measurements and environment shown the color-color space. Each point in the plot is shown at the mean colors in each of the bins we use. The grey value or color of the points in each panel show the mean value in each bin for the quantity described by the corresponding color bar. *Top left:* Logarithmic number density in each of the bins; all bins with less than 5 galaxies were discarded in this and the other panels. *Top right:* Environment; in each bin, the average number of nearest neighbors is calculated in a projected cylinder ($r_t = 0.5\mathcal{M}pc$ and $v_{los} = \pm 1000 km/s$). *Bottom left:* the Specific Star Formation Rates obtained from MAGPHYS. *Bottom right:* UV Specific Star Formation Rates estimated by using the method described in Salim et al. (2007a).

1.4.2 Edge Effects

We must also account for the survey edges. For galaxies at the edge, part of the fixed aperture used to estimate the environments might lie outside the survey coverage. It is important to identify these galaxies and either discard them or assign an appropriate weight to $n_{\rm env}$ in order to account for the missing area.

To identify the edges, we use (Swanson et. al.'s) `Mangle`, a suite of free open-source software designed to deal with complex angular masks in an efficient and accurate manner. First, the NYU-VAGC `Mangle`-format mask was used to obtain the angular mask for the NASA Sloan Atlas by using the *polyid* routine from `Mangle`. Then, the *ransack* routine was used to populate the mask with a random sample of $N = 10,000,000$ galaxies. For each galaxy, we compute the angular separation ϑ_i that corresponds to our $0.5 Mpc$ aperture at the redshift of that galaxy. We then count the number of galaxies n_i that lie within this angular separation and compare the value obtained to the expected value:

$$\left\langle n \right\rangle_i = \frac{N}{A_{\rm EDP}} \times \pi \vartheta_i^2 \times f_{\rm thresh}$$

$A_{\rm EDP}$ is the total area of the mask and $f_{\rm thresh}$ is the fractional threshold for the edge effect cut-off. In our case, we chose $f_{\rm thresh} = 0.8$. Wherever $n_i < \left\langle n \right\rangle_i$, we consider the galaxy to be near an edge and discard it from our sample.

1.4.3 Environments in Color-Color Space

The mean environment, quantified by $(\langle n_{\rm env} \rangle + 1)$ in each bin are shown in the upper right panel of Fig. 1.2 as a function of optical and infrared colors. As we expect from many pre-

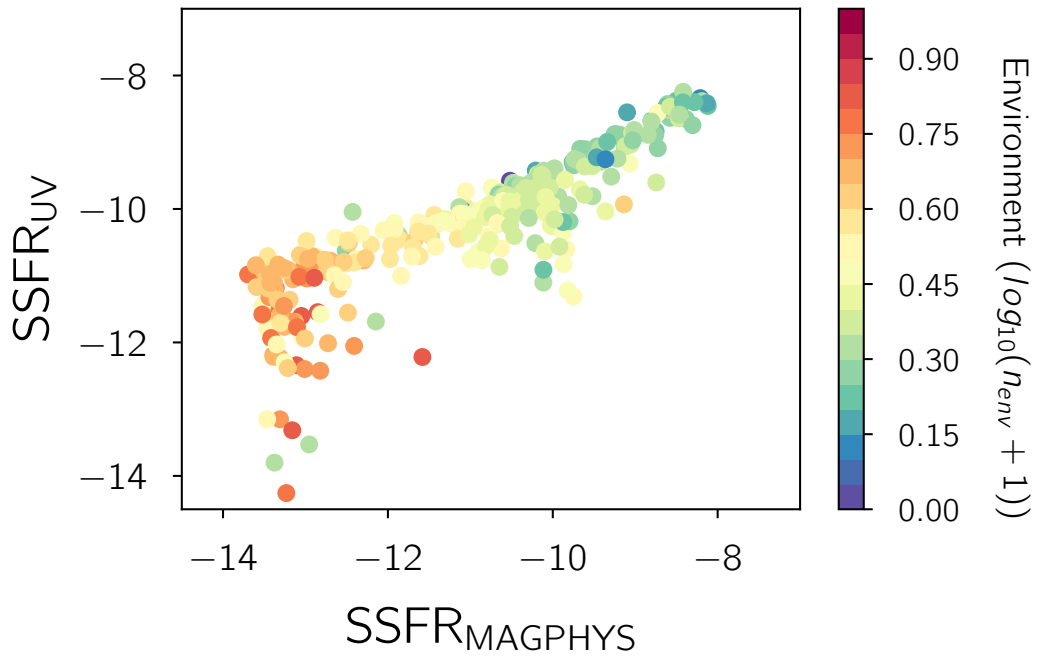

Figure 1.3: The two star formation rate estimates (from Fig.1.2) plotted against each other as a function of the environment; We notice two distinct set of outliers that seem to have lower UV SSFR's but similar environments to the galaxy bins with the same MAGPHYS SSFR's.

vious studies (Blanton & Moustakas 2009b) the star-forming bluer galaxies tend to exist in less dense environments on average and the red-and-dead population tends to exist in more dense environments. In the UV-optical green valley region ($3 < N - r < 5$) there is some indication that the environment declines with $[W1] - [W3]$ color at fixed UV-optical color. However, the mean environments in this plot cannot easily be interpreted, because the mean stellar mass in each bin is different, so some of the variation is driven by the dependence of environment on stellar mass.

1.5 The Environments of the Outliers

Fig. 1.3 shows the relationship between the two SSFR measurements, with points colored according to the mean environment, for each bin in color-color space from Fig. 1.2. There is a set of bins in the range $-10.5 < \mathrm{SSFR}_{\mathrm{MAGPHYS}} < -9.5$ that have lower $\mathrm{SSFR}_{\mathrm{UV}}$ values than the general trend, and have environments similar to the other galaxy bins in the same MAGPHYS range. Hereafter we shall refer to this population as the "Outliers," to distinguish them from the general trend line in Fig. 1.3.

We identify these outliers more specifically in Fig. 1.4(a), as being in the lower right square. The galaxy bins with the same $\mathrm{SSFR}_{\mathrm{MAGPHYS}}$ values (above the square) are identified as the "MAGPHYS Box" and the bins with the same $\mathrm{SSFR}_{\mathrm{UV}}$ values (left of the square) are identified as "UV BOX" in Fig. 1.4(a).

.. change line styles of different boxes in Fig.1.5 so that the result can be inferred on b-and-w print...

1.5.1 Green-valley interlopers

When we return to the color-color space (Fig. 1.4(b)) and show where the bins in each box lie, we see the trends we would expect. The Outliers lie in a similar UV-optical color range as the UV box but have higher IR color. The MAGPHYS Box occupies the bluer side in the optical color range while spanning almost the entire IR color range. The UV Box occupies the redder side in the optical color range while having lower IR color values. The Outlier bins are the same bins we previously identified as the galaxies in the UV-optical "green valley" that are there due to dust reddening.

To verify this, we unwrap the bins and look at the Probability Density Function of the

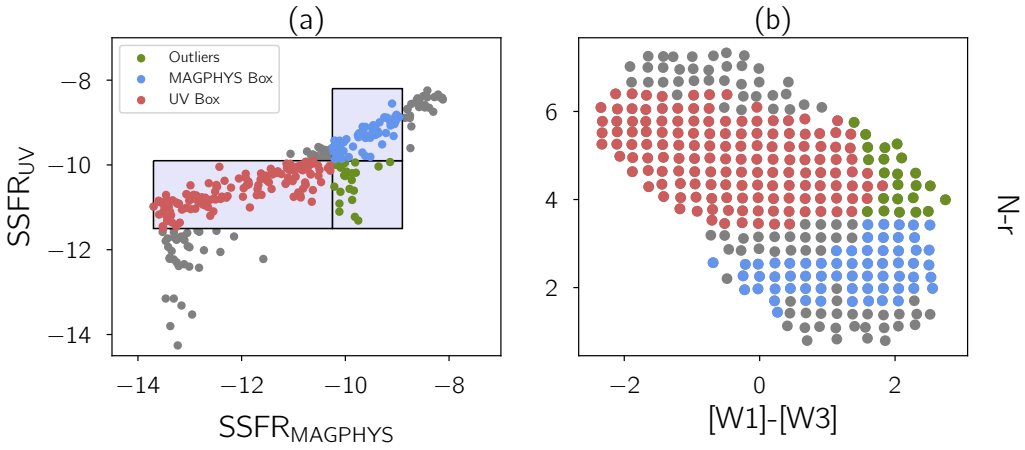

Figure 1.4: The outliers shown as a function of the Star Formation Rates as well as Optical and IR colors

Environments of the galaxies in these three regions in the mass range $9.5 < \mathcal{M}_* < 10.7$ and examine the distribution of environments in these three regions, the result of which is plotted in Fig. 1.5.

1.5.2 Jackknife Errors

To calculate uncertainty in the estimated probability density functions of the environments, $P_{i,\mathrm{bin}}$'s : $i = 1, 2, 3$ for each of the populations, we use the standard jackknife technique. Jackknife re-sampling gives us an internal error estimate that tests how representative a measurement/trend is of the data it is estimated with. We divide our entire sample into 20 subsamples with nearly equal co-moving volumes and estimate the same probability density functions(P_i^j's) for the whole sample while leaving out one subsample each time. We can then estimate our uncertainty for each bin in the PDF's thus:

$$\sigma_{i,\mathrm{bin}} = \sqrt{\frac{N}{N-1}\sum_{j=1}^{j=N}(P_i^j - P_{i,bin})^2}$$

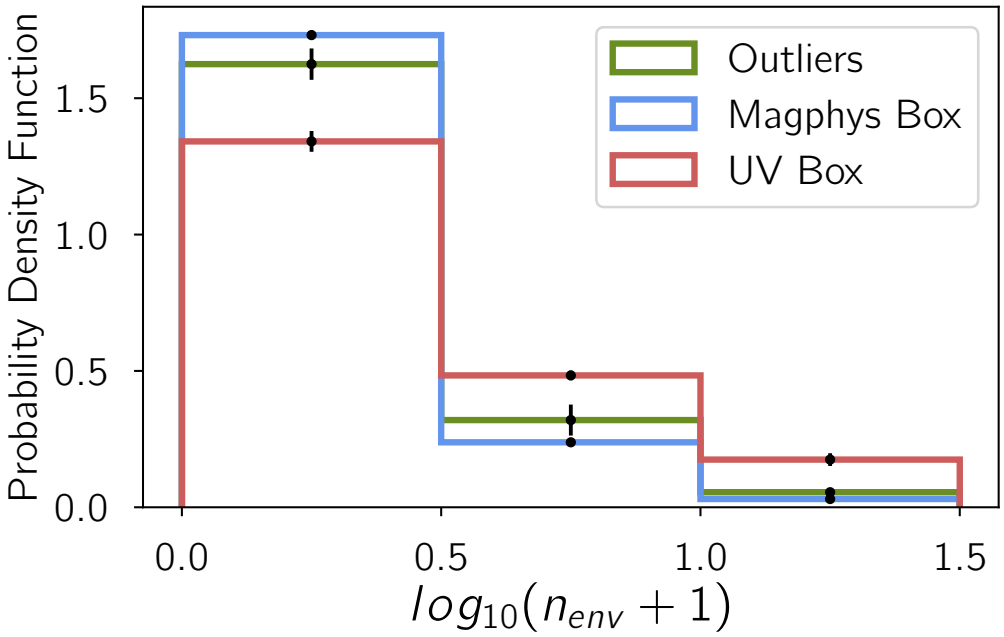

Figure 1.5: Probability density functions of the Environments of the three populations described in Fig. 2

The errors estimated in this manner account for Poisson shot noise and also the sample variance, the extra error associated with the fact that the density field varies across the survey. Although precision studies of large scale structure have found that latter effect is not perfectly accounted for with standard jackknife techniques, they are precise enough for our purposes here. The jackknife errors are shown in Fig. 4 and confirm our hypothesis: that the Outliers are a little different than the MAGPHYS Box but still, very different from the UV Box.

1.6 Summary and Conclusion

- From Fig 1, we see that $SSFR_{MAGPHYS}$ identifies a region in the color-color space as

dust-obscured star forming galaxies and correlates better with the environments of the galaxies.

- At the higher star formation end, we find that the dust-obscured star-formers as identified by MAGPHYS have environments comparable to the blue star-forming galaxies, confirming that this is indeed a physical effect we're seeing.

- Comparing the environment distribution of the Outliers relative to the galaxies with (a) the same $SSFR_{MAGPHYS}$'s as the Outliers and (b) the same $SSFR_{UV}$'s as the Outliers (Fig. 1.5), we find that the Outliers indeed have a similar environment distribution to the galaxies that have the same $SSFR_{MAGPHYS}$'s, i.e., they seem to favor lower environment densities mimicking the behavior of star-formers.

2

Aperture effects in Stellar Mass Estimates

2.1 Introduction

In this chapter we investigate methods of constraining the star formation histories and stellar masses of galaxies where galaxy spectra are available. In particular, we look at the largest galaxy catalog of estimated stellar masses, star formation rates and gas metallicities (the MPA-JHU catalog; NEED CITATION) obtained for the Sloan Digital Sky Survey (SDSS) Legacy Survey. The MPA-JHU catalog has, over the last decade and a half, been one of the most influential and widely-used catalogs in the fields of galaxy formation and evolution. Here we test a fundamental assumption of the catalog, which is that spectroscopic measurements of the central region of the galaxy yield sufficient information to constrain star formation histories and stellar masses for the galaxy as a whole.MRB says: You need to describe briefly why we want to measure these quantities. Call back to Chapter 0.

The SDSS spectra are obtained for multiple objects at a given time. This is done by connecting the spectrographs to fiber optic cables which are plugged into an aluminum plate that is placed in the telescope's focal plane. These optical fibers have a fiber diameter of 3″. Thus for each galaxy in the SDSS, while photometry is available for the entire galaxy, spectra are available only for the region of the galaxy contained within this 3″ angular aperture. Thus, the fraction of the galaxy falling within the aperture may vary widely with the redshift of this galaxy. I describe below how the MPA-JHU catalog approached this problem.

The stellar masses and star formation histories in the catalog are obtained by looking at two key spectral indicators of starbursts and age of a galaxy: the Balmer $H\delta_A$ absorption line index and the D_n4000 break index, both of which are relatively insensitive to the metallicity-age degeneracy issue that spectral indicators in the redder side of the spectrum

are limited by. Because they are both measurements over a narrow range of wavelengths, that are similar to each other, and are independent of the absolute flux, they are designed to be insensitive to dust extinction within the galaxy. Using the distribution of the observed galaxies in the $H\delta_{\rm A} - D_n4000$ plane and by employing Stellar Population Synthesis (SPS) models by Bruzual & Charlot (2003b) to model the evolution of galaxies in this plane, they are able to infer a mass-to-light ratio in the z-band (Kauffmann et al., 2003) for every point in this phase space. From here, it is a short step to using the luminosity of the entire galaxy to infer the stellar mass and star formation history of the galaxy.

However, this methodology can be problematic when the mass-to-light ($\mathcal{M}/L$) ratio of the central part of a galaxy is not representative of the entire galaxy. This can be an issue where there are distinct bulge and disk components, such as for luminous spiral galaxies. However, with the availability of spatially resolved spectra for galaxies from IFU (Integral Field Unit) based surveys such as MaNGA(Mapping Nearby Galaxies at Apache Point (Bundy et al., 2014)), SAMI (Sydney-Australian-Astronomical-Observatory Multi-object Integral-Field Spectrograph (Bryant et al., 2015)), MUSE (Multi Unit Spectroscopic Explorer (Bacon et al., 2015)) and CALIFA (Calar Alto Legacy Integral Field Area Survey) (Sánchez et al., 2012), we can actually put this question to the test and quantify the effect of aperture size on the SDSS stellar masses. We use MaNGA, the largest IFU-based survey thus far, which is based on SDSS, and ask the following questions: At any given redshift in the local Unverse, how does the position of the galaxy in the $H\delta_A - D_n4000$ plane as measured using a 3″ aperture compare to using a full aperture, i.e. spectra from all the spatially resolved regions in the galaxy.

2.1.1 The SDSS spectra

Describing the SDSS spectrograph and 3″ fiber diameter. References: (Smee et al., 2013) (York et al citation).

The galaxy spectra in SDSS are obtained through 3″ diameter fibers. The rest-frame wavelength range of the spectra at the median redshift is from 3500 Åto 8500 Åwith a spectral resolution

$$R = \frac{\Delta\lambda}{\lambda} \approx 2000$$

. The spectra are calibrated using observations of F stars in each 3 degree field.

2.1.2 The MPA JHU Catalog

Introduction to and describing the importance of the largest catalogue of galaxy stellar masses (Kauffmann et al., 2003), star formation rates (Brinchmann et al., 2004) and gas metallicities (Tremonti et al., 2004) thus far. Including major results that rely on said SFR's.

MRB says: Then you need to mention some major results that depend on the MPA-JHU catalog measurements of this quantity, just a couple of highlights from the later section. TBD: Kewley et al 2006 (host galaxies of AGN's); Elbaz et al 2007 The reversal of the star formation-density relation in the distant universe; Kewley 2008 Metallicity Calibrations and the Mass-Metallicity Relation for Star-forming Galaxies; Peng et al 2010(mass and environments as drivers etc); Kauffmann 2013 A re-examination of galactic conformity and a comparison with semi-analytic models of galaxy formation.

.....

The MPA-JHU catalog was developed as a result of a joint collaboration between MPA

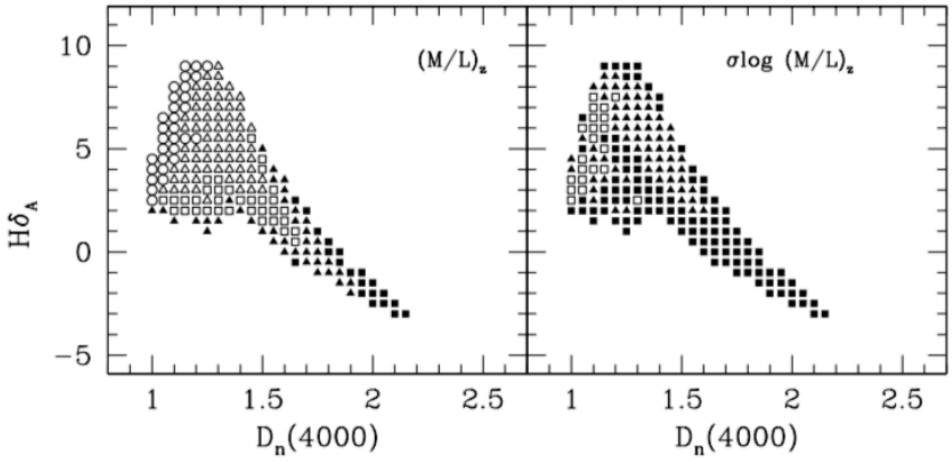

Figure 2.1: The Kauffmann et al. (2003) grid to infer M/L ratios from the $h\delta_A - D_n4000$ plane

and JHU right after the SDSS Data Release 1(DR1) of spectroscopic observations. Using the previously mentioned spectral indicators (D_n4000 and $H\delta_A$) and broadband photometry from SDSS, they developed a method to derive maximum likelihood estimates of the stellar mass of a galay, the attenuation of optical light by dust and the fraction of stars in a galaxy formed in recent bursts. The dataset they used was 120,808 galaxies drawn from the SDSS DR1.

2.2 The $H\delta_A - D_n4000$ plane

Two powerful spectral diagnostic tools that are valuable in constraining stellar masses and star formation histories in galaxies are the Balmer δ absorption line index and the D_n4000 break index in the optical spectrum of a galaxy (Kauffmann et al., 2003). One of the key issues in spectral indicators for starbursts is the existence of the age-metallicity degeneracy in stellar populations (Worthey, 1994). The heavier element lines are often prominent in

both early type as well as metal rich galaxies and the two are hard to distinguish in terms of interpretation as older stellar populations exhibit metal richness as well and without accurate modeling of the chemical evolution of galaxies, it is difficult to ascertain the reason. The Balmer $H\alpha$ and $H\beta$ are sensitive to the effects of metallicity as well. However both the Balmer $H\delta$ absorption line as well as the D_n4000 break occurring in the continuum are both in a bluer region of the spectrum relatively unaffected by metallicity constraints and together they form a powerful diagnostic tool to constrain the mass-to-light ratios of galaxies.

2.2.1 Measuring the D_n4000 index

The most obvious discontinuity in the spectrum of a galaxy is often the D_n4000 break (Balogh et al., 1999), which is a consequence of the absorption into electronic excited states by neutral and partially ionized metals whose lines happen to overlap in the region just blueward of 4000 Å. Older stellar populations have spectra dominated by relatively cool giant stars, and under these conditions the partially ionized metal lines are strong. Younger stellar populations have spectra dominated by hot stars, for which these lines are weaker. In addition the break depends on stellar metallicity, exhibiting some of the same age-metallicity degeneracy that afflicts most spectroscopic indicators.

This break was defined in by Bruzual A. (1983) as the ratio of the average flux density F_ν in two bands that span ~200 Åon either side of 4000 Å. Balogh et al. (1999) defined a narrow band definition for the same where the bands that are now 100 Åwide with 3850 Å-3950 Åas the "blue continuum" and 4000 Å- 4100 Åas the "red continuum". The bandpass used in Kauffmann et al. (2003) (2.2) is the same as the one introduced by Balogh et al.

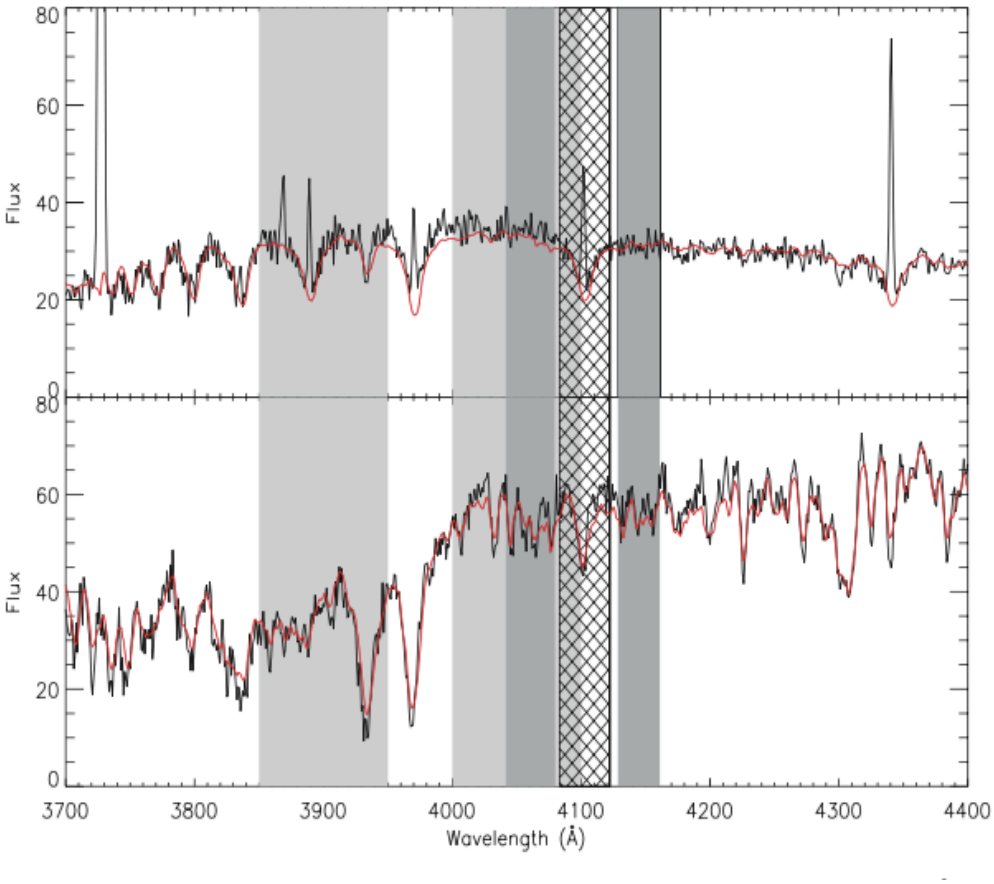

Figure 2.2: PLACEHOLDER FIG; TBD: A figure showing D4000 and Hdelta breaks in spectra for early/late-type galaxies as well as the bimodality in D4000

(1999) and their motivation for doing so is that the narrow definition is more insensitive to reddening effects. I reproduce these measurements using the same narrow band definition.

2.2.2 Measuring the $H\delta_A$ index

2.3 Manga Overview

Citations: (Bundy et al., 2014)

2.3.1 Introduction to Integral Field Spectroscopy

What is Integral Field Spectroscopy? What is an Integral Field Unit?

2.3.2 The MaNGA IFU Design

What is a spaxel? (Drory et al., 2015)

2.4 Data

2.4.1 MaNGA Target Selection and DRP

Primary and Secondary Samples. NSA redshifts/Luminosity cut.

2.4.2 Our Sample

The most recent MaNGA product launch, MPL-8, which was announced in November 2018, containing products based on galaxy and stellar library observations from March 2014 - July 2018 serves as the source of our sample. It contains 950 plates - 6779 data cubes and 20649 stellar library stars. Out of these, 6468 are galaxies with measured NSA redshifts.

These are representative of all the IFU sizes (list them: 19,37... 127) and span a redshift range upto $z = 0.15$.

For each galaxy observation, depending on the IFU bundle size (say N_X, N_Y each describing a position 0.5" from the previous spaxel), we have (N_X, N_Y) spectra which span 4563 wavelength points.

2.5 Methods

2.5.1 Variable Aperture Measurements

For any given datacube, we can determine which spaxels fall within an aperture radius of R arc-seconds as follows. As each spaxel spans a width of 0.5" in along the "X" and "Y" direction, at any point (x, y) in the IFU image, the distance in arc-seconds of the centre of a spaxel from the central spaxel (x_c, y_c) in the IFU would be:

$$d = (r(x, y) - r(x_c, y_c)) = \sqrt{(0.5 * x)^2 + (0.5 * y)^2}$$

Thus, for every spaxel in the IFU, where $d <= R$, that part of the galaxy would fall within the aperture and hence, we would include that spaxel in the measurement of whichever spectral index. Using this, for instance, we can simulate the SDSS fiber measurement, i.e., what the 1.5" aperture radius used in SDSS would see versus the total galaxy or what we call a "full aperture" measurement.

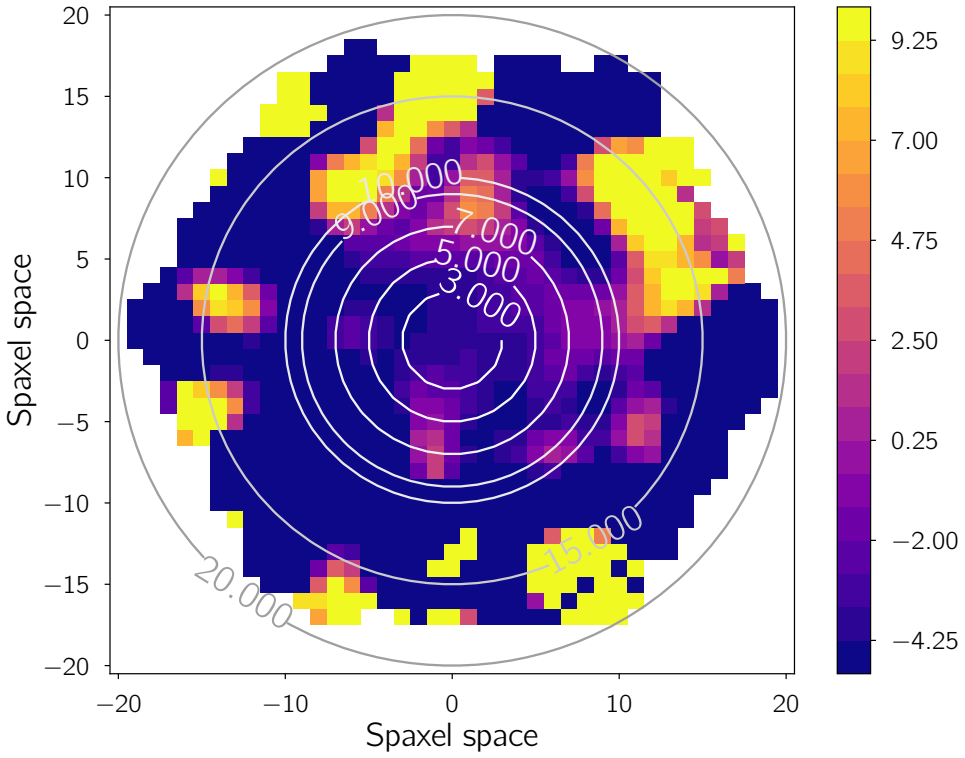

Figure 2.3: Placeholder figure: TBD. Sample MaNGA galaxy view in the spaxel space with the H_{α} distributions plotted as a function of position and the contours marking the aperture diameters at different angular distances in arcseconds

2.5.2 Variable Redshift Measurements

One can alternately pose this question in terms of redshift. For all galaxies whose redshift z_{obs} is less than the redshift we are interested in, z_{cutoff}, we can ask the question: if we shift the said galaxy to the said cutoff point, where would its location on the $H\delta_{\text{A}}$ - $D_{\text{n}}4000$ plane be? How offset is this from the "full aperture" measurements?

Transverse angular distance varies with redshift as follows:

$$D_{\text{A}}(z) = \frac{D_{\text{M}}(z)}{1+z}$$

, where $D_{\text{M}}(z)$ is the co-moving distance at redshift z.

So when a galaxy at z_{obs} is shifted to z_{cutoff} the new distance d_{new} of spaxel (x, y) from the central spaxel (x_c, y_c) relates to the old distance thus:

$$d_{\text{new}} = \frac{(1+z_{\text{cutoff}}) \times D_{\text{M}}(z_{\text{obs}}) \times d}{(1+z_{\text{obs}}) \times D_{\text{M}}(z_{\text{cutoff}})}$$

Using the above, we can now figure out the spaxels that would fall within a 3" diameter aperture (say) at not only the observed redshift but also any redshift where we would like to collectively observe the behavior of the offset with a full aperture measurement in the $H\delta_{\text{A}}$ - $D_{\text{n}}4000$ plane.

2.5.3 $H\delta_{\text{A}}$, $D_{\text{n}}4000$ Measurements within Apertures

To get the $H\delta_{\text{A}}$ and $D_{\text{n}}4000$ index measurements for any aperture, we first redshift-correct the spectra obtained from all the spaxels within the aperture to rest-frame. As both the

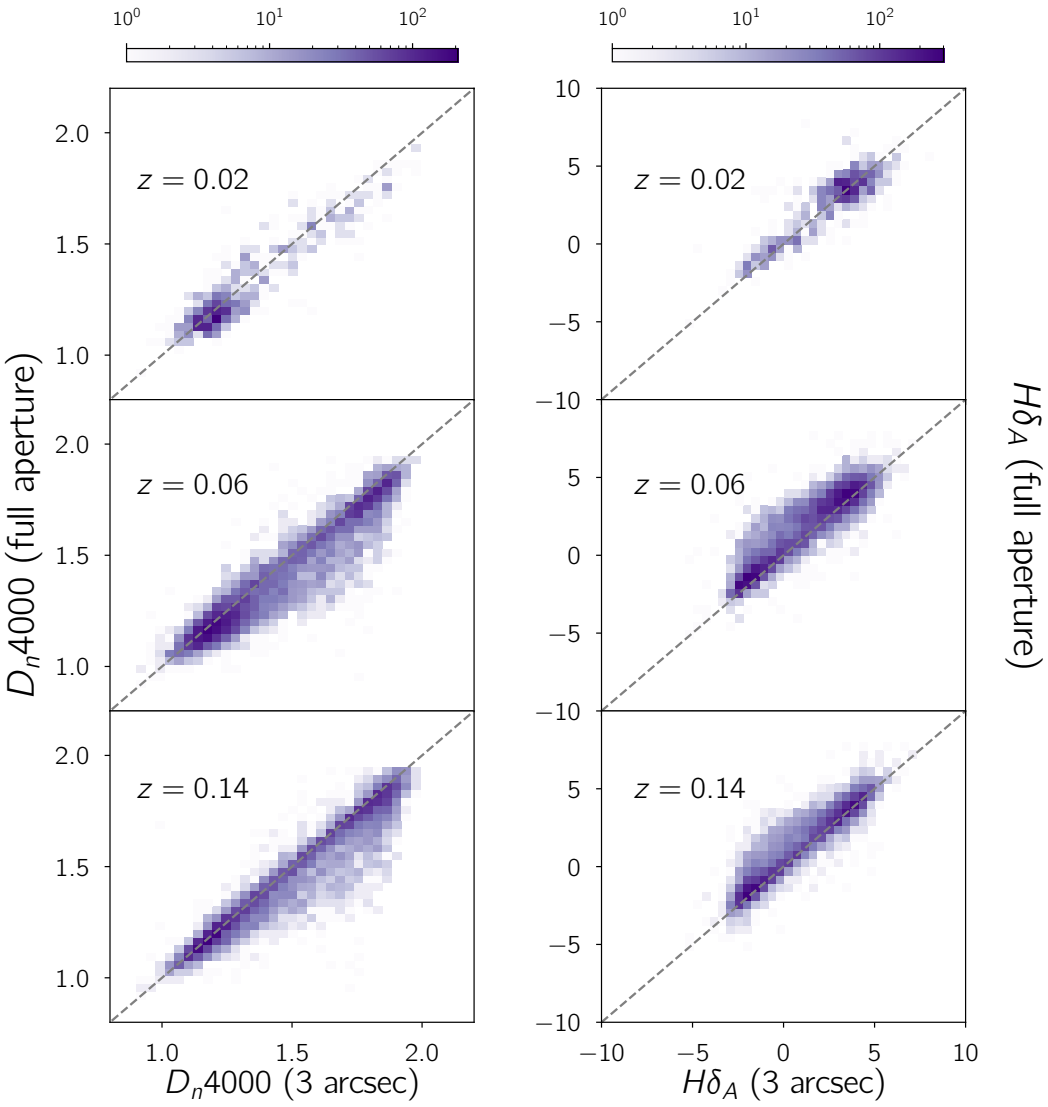

Figure 2.4: The D_n4000, $h\delta_A$ indices measured at $z = 0.02, 0.06, 0.14$ with a $3''$ aperture compared to the full aperture measurement

equivalent width of the Balmer $H\delta$ line as well as the D_n4000 break rely on the continuum as well as a ratio of fluxes in the case of the latter, we add up the spectra of the spaxels that fall within any aperture before estimating either. We then follow the procedure described in Section 2.2 to calculate the indices. (In a footnote: the code for this is publicly available at –provide github link–.)

2.6 Comparison to Full Aperture Measurements

To investigate how the full aperture measurements compare to the 3" measurements, we choose 3 different redshift bins $z = 0.02, 0.06$ and 0.14 and observe how offset the $H\delta_A$ and D_n4000 measures are. For each redshift, I pick the galaxies whose redshift are below that redshift and "shift" them to the cutoff redshift as described in Section 2.5 and compare the full aperture measurements to the 3" measurements made at that redshift. The results of this are shown in Fig. 2.4, where the full aperture measurements are plotted against the 3" measurements at the respective redshifts with the colorbars indicating the number of galaxies in each bin. We note that the total number of galaxies in each redshift bin is 561 for $z = 0.02$, 5016 for $z = 0.06$ and 6402 for $z = 0.14$.

From Fig. 2.4, we can infer the following. For most of the galaxies the offset is pretty minimal as it as they fall pretty close to the $x = y$ line. We find that the scatter is the most at $z = 0.06$ and tends towards higher D_n4000 and lower $H\delta_A$ values relative to the full aperture measurements. This can be interpreted as the effect of the apertures beginning to cover the galaxy disks which have lower star formation activity than the bulge for galaxies with strong bulges. The scatter lessens as we approach $z = 0.14$, close to the survey limit, where for most of the galaxies, all of the light gets accounted for by the 3"aperture at this

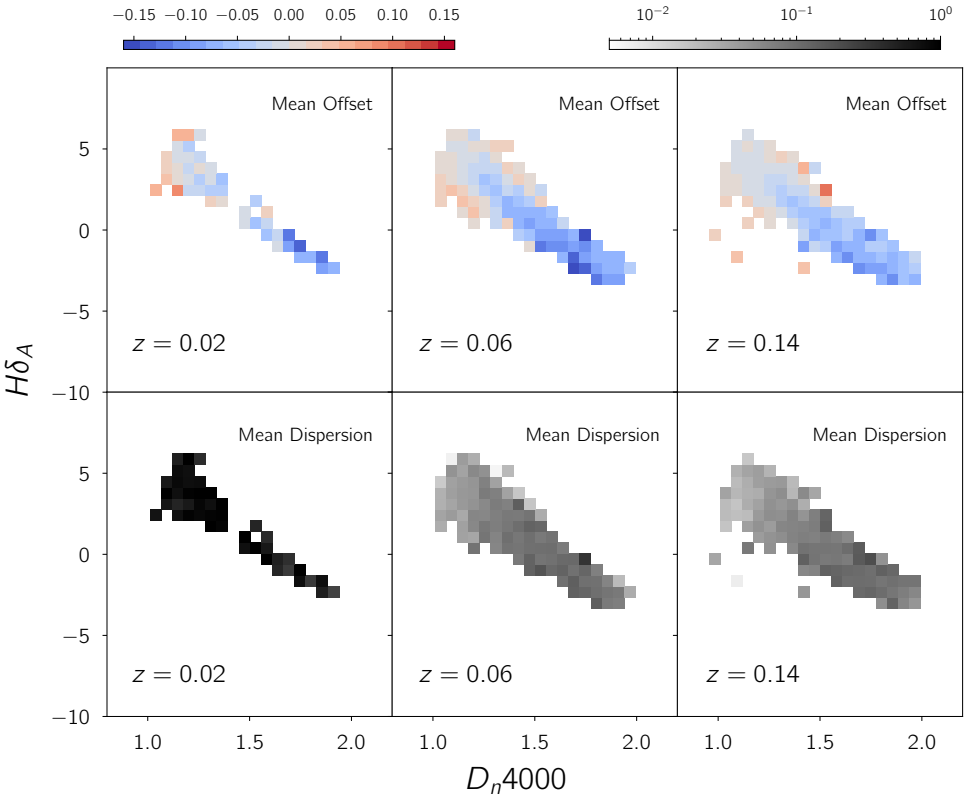

Figure 2.5: The mean offset and dispersion in the D_n4000 index measured at $z = 0.02, 0.06$ and 0.14 with a $3''$ aperture from the full aperture measurement

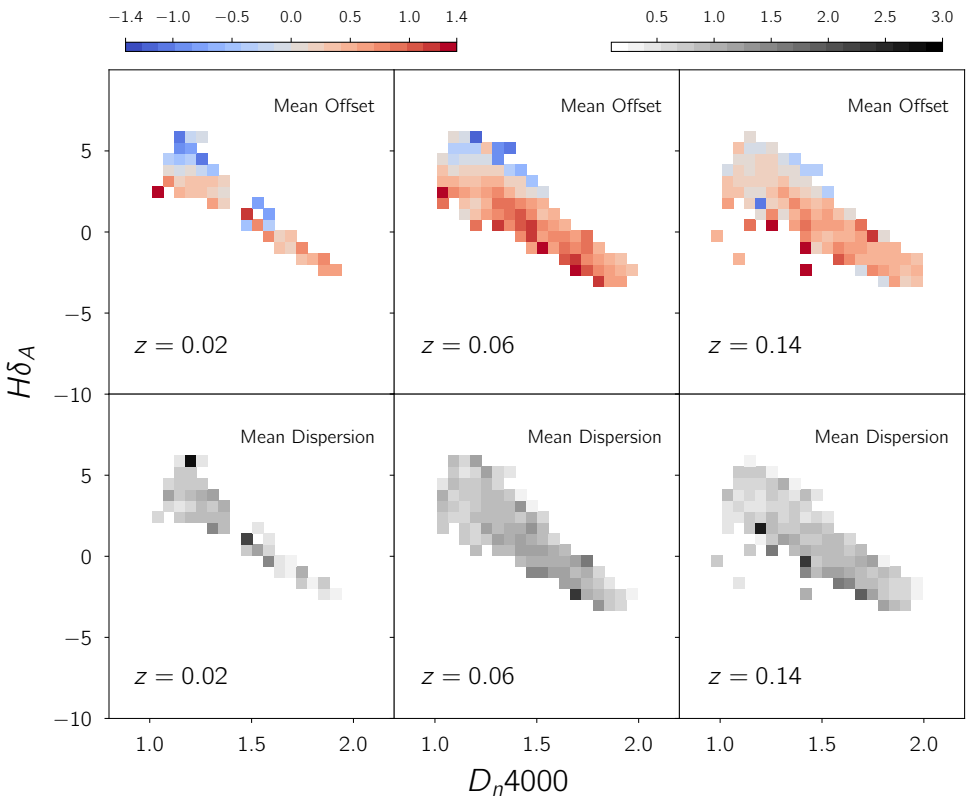

Figure 2.6: The mean offset and dispersion in the $h\delta_A$ index measured at $z = 0.02, 0.06$ and 0.14 with a $3''$ aperture from the full aperture measurement

point.

MRB Says: At all redshifts, we can see that there is a systematic tendency for galaxies to appear older through the fiber aperture than through the full aperture, and therefore to appear to have a higher M/L than they actually do. This would particularly affect the intermediate age galaxies (i.e. those with D_n4000 in the green valley).

2.7 Offsets in the $H\delta_A$-D_n4000 plane

2.8 Discussion

MRB Says: * This mean tendency is *relatively* small. You should calculate from your grids the median offset for cells with D4000 > 1.3 or something like that, and quote that number. You should then look carefully at the Kauffmann figure to translate this to a change in $\mathcal{M}/L_z$ — my guess is that it is around 0.1 dex for z=0.06. Do this for z=0.06 and z=0.14.

* The scatter about this mean is substantial relative to the mean. Again, calculate the median standard deviation over the cells with D4000 > 1.3 to quantify this. My guess is that it is comparable to the mean itself. This means for individual galaxies the error can be a lot bigger. Again quote for both those redshifts.

* The main conclusion is that stellar masses more accurate than 0.1 dex (or whatever you see in the mean offset) are not possible, and that the scatter in the offset means the precision is degraded as well. This source of error is important to keep in mind but is probably not fatal for samples at z=0.1 from MPA/JHU — most results done rely on stellar masses at that precision. Using this sample at lower redshift may be much more iffy.

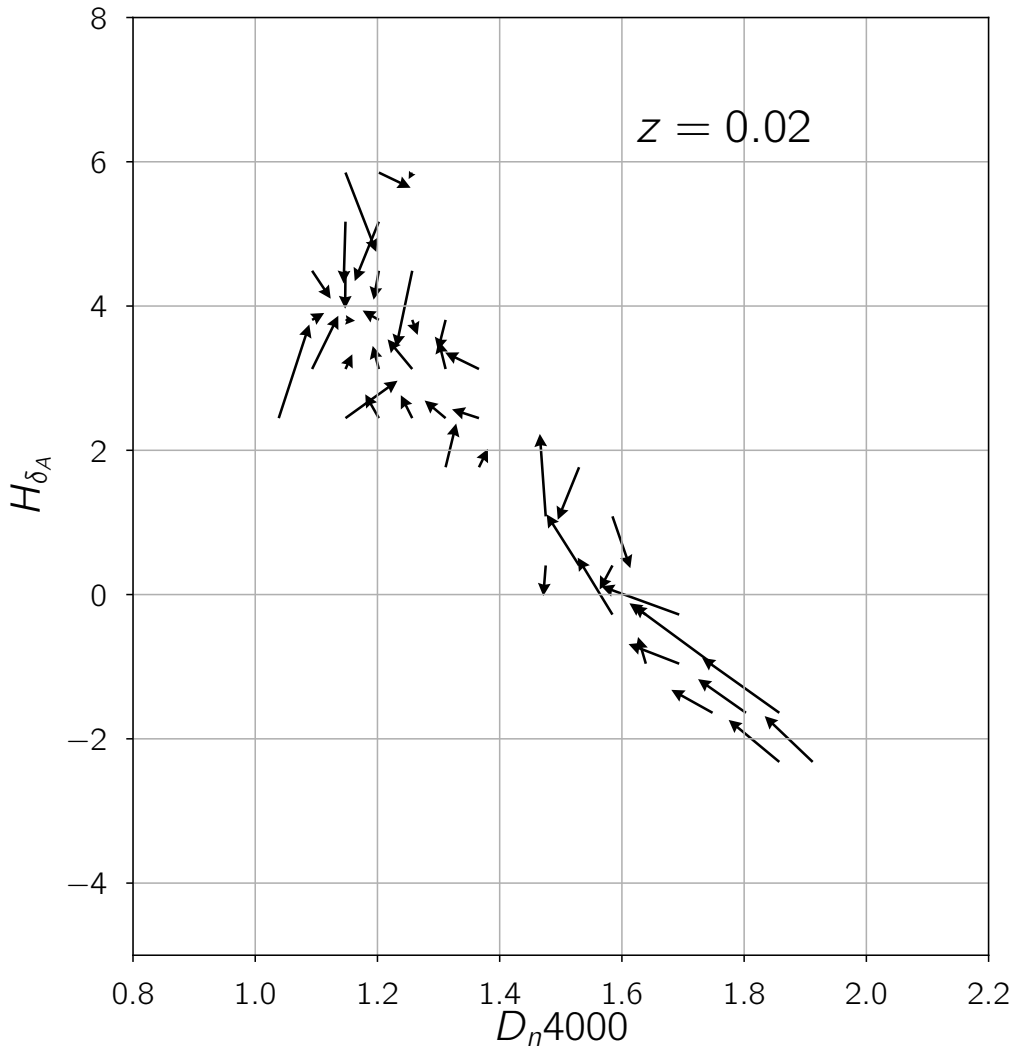

Figure 2.7: The combined mean offset in $D_{\rm n}4000$-$h\delta_{\rm A}$ at $z = 0.02$ from the full aperture measurements represented as a vector whose projections on the axes are the actual offsets in either direction

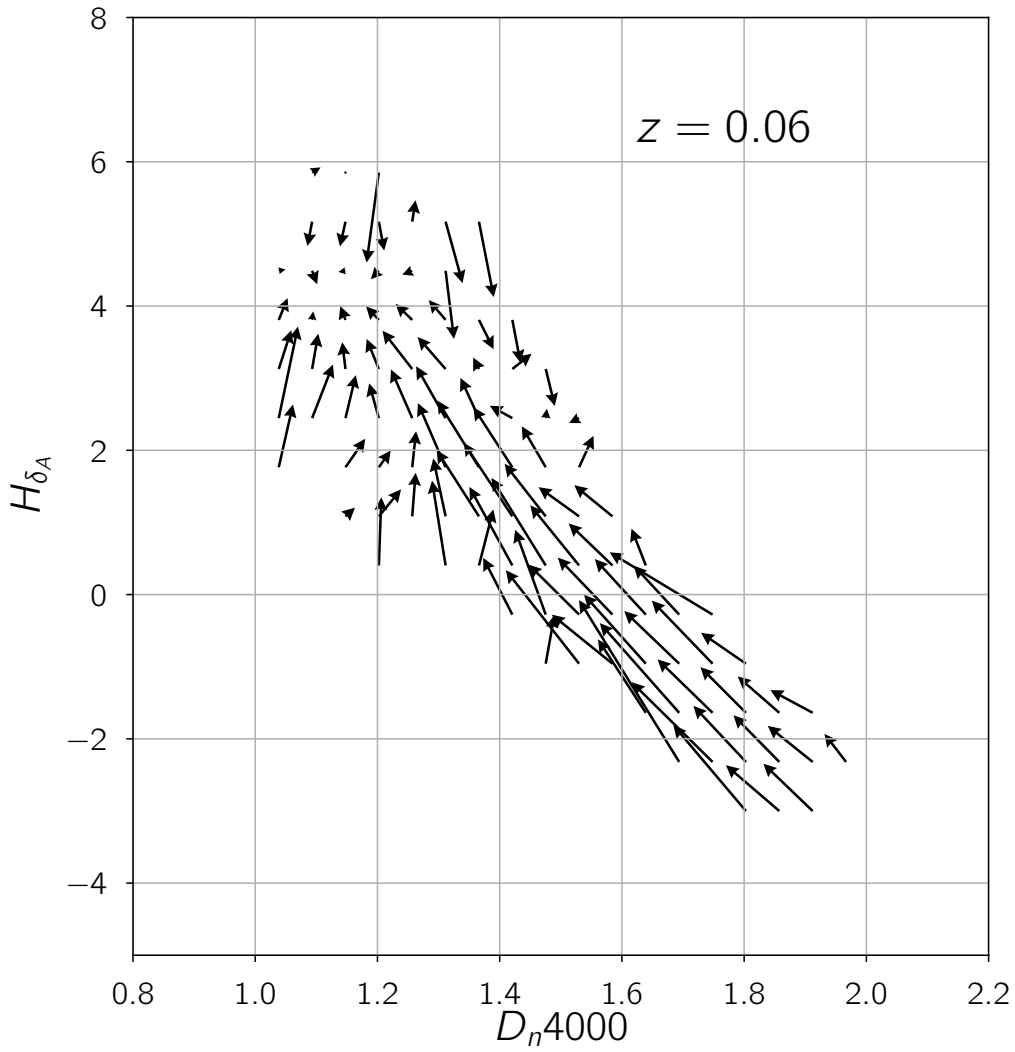

Figure 2.8: The combined mean offset in $D_{\rm n}4000$-$h\delta_{\rm A}$ at $z = 0.06$ from the full aperture measurements represented as a vector whose projections on the axes are the actual offsets in either direction

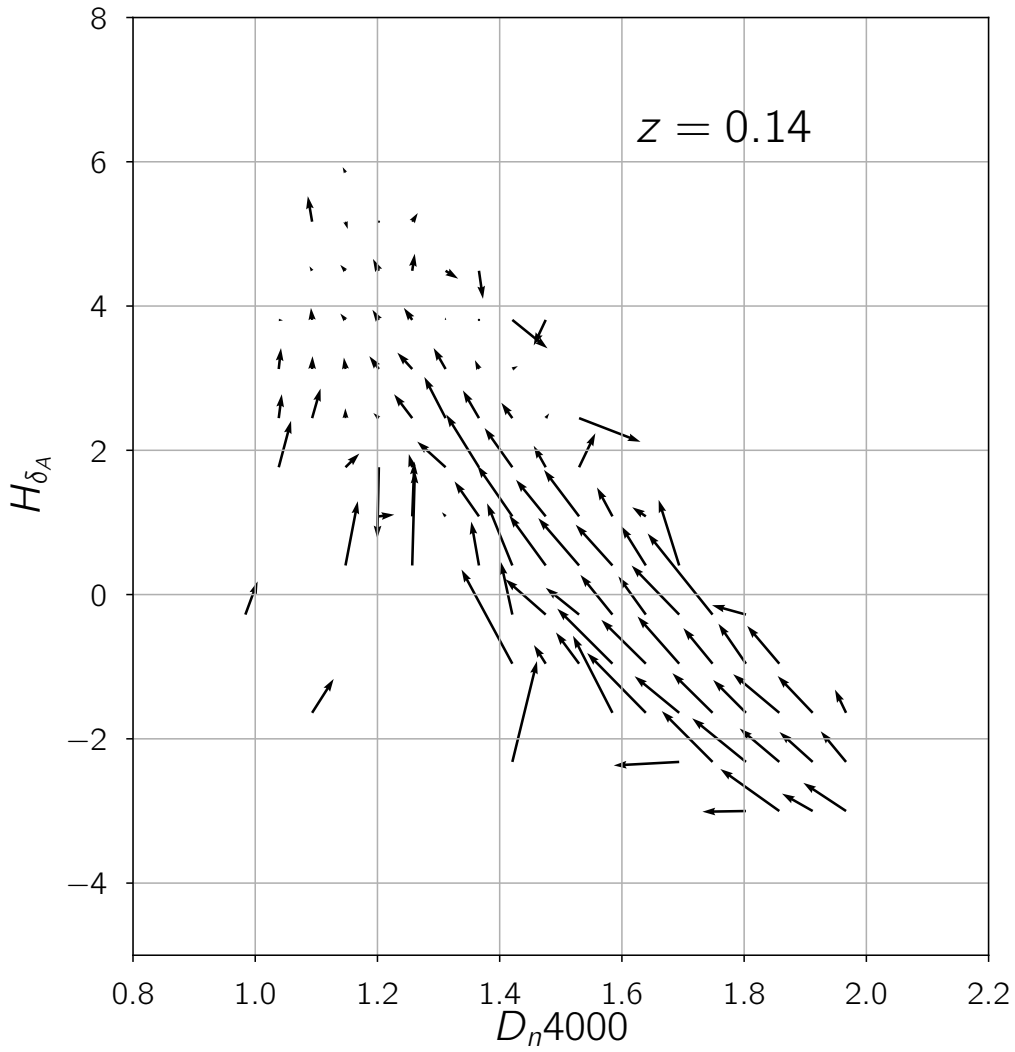

Figure 2.9: The combined mean offset in $D_{\rm n}4000$-$h\delta_{\rm A}$ at $z = 0.14$ from the full aperture measurements represented as a vector whose projections on the axes are the actual offsets in either direction

3

Conclusion

References

Agertz, O., Moore, B., Stadel, J., Potter, D., Miniati, F., Read, J., Mayer, L., Gawryszczak, A., Kravtsov, A., Nordlund, Å., Pearce, F., Quilis, V., Rudd, D., Springel, V., Stone, J., Tasker, E., Teyssier, R., Wadsley, J., & Walder, R. (2007). Fundamental differences between SPH and grid methods. *some journal name*, 380, 963–978.

Alpher, R. A., Bethe, H., & Gamow, G. (1948). The Origin of Chemical Elements. *Physical Review*, 73(7), 803–804.

Bacon, R., Brinchmann, J., Richard, J., Contini, T., Drake, A., Franx, M., Tacchella, S., Vernet, J., Wisotzki, L., Blaizot, J., Bouché, N., Bouwens, R., Cantalupo, S., Carollo, C. M., Carton, D., Caruana, J., Clément, B., Dreizler, S., Epinat, B., Guiderdoni, B., Herenz, C., Husser, T.-O., Kamann, S., Kerutt, J., Kollatschny, W., Krajnovic, D., Lilly, S., Martinsson, T., Michel-Dansac, L., Patricio, V., Schaye, J., Shirazi, M., Soto, K., Soucail, G., Steinmetz, M., Urrutia, T., Weilbacher, P., & de Zeeuw, T. (2015). The MUSE 3D view of the *Hubble* Deep Field South. *Astronomy & Astrophysics*, 575, A75.

Balogh, M. L., Morris, S. L., Yee, H. K. C., Carlberg, R. G., & Ellingson, E. (1999). Differential Galaxy Evolution in Cluster and Field Galaxies at z˜0.3. *some journal name*, 527, 54–79.

Behroozi, P. S., Conroy, C., & Wechsler, R. H. (2010). A COMPREHENSIVE ANALYSIS OF UNCERTAINTIES AFFECTING THE STELLAR MASS-HALO MASS RELATION FOR 0 < *z* < 4. *The Astrophysical Journal*, 717(1), 379–403.

Bell, E. F. & de Jong, R. S. (2001). Stellar Mass-to-Light Ratios and the Tully-Fisher Relation. *some journal name*, 550, 212–229.

Blanton, M. R., Eisenstein, D., Hogg, D. W., & Zehavi, I. (2006). The Scale Dependence of Relative Galaxy Bias: Encouragement for the "Halo Model" Description. *some journal name*, 645, 977–985.

Blanton, M. R., Hogg, D. W., Bahcall, N. A., Baldry, I. K., Brinkmann, J., Csabai, I., Eisenstein, D., Fukugita, M., Gunn, J. E., Ivezić, Ž., Lamb, D. Q., Lupton, R. H., Loveday, J., Munn, J. A., Nichol, R. C., Okamura, S., Schlegel, D. J., Shimasaku, K., Strauss, M. A., Vogeley, M. S., & Weinberg, D. H. (2003). The Broadband Optical Properties of Galaxies with Redshifts 0.02<z<0.22. *some journal name*, 594, 186–207.

Blanton, M. R., Lupton, R. H., Schlegel, D. J., Strauss, M. A., Brinkmann, J., Fukugita, M., & Loveday, J. (2005). The Properties and Luminosity Function of Extremely Low Luminosity Galaxies. *some journal name*, 631, 208–230.

Blanton, M. R. & Moustakas, J. (2009a). Physical Properties and Environments of Nearby Galaxies. *Annual Review of Astronomy and Astrophysics*, 47(1), 159–210.

Blanton, M. R. & Moustakas, J. (2009b). Physical Properties and Environments of Nearby Galaxies. *Annual Review of Astronomy and Astrophysics*, 47(1), 159–210.

Blanton, M. R. & Roweis, S. (2007). K-Corrections and Filter Transformations in the Ultraviolet, Optical, and Near-Infrared. *some journal name*, 133, 734–754.

Brinchmann, J., Charlot, S., White, S. D. M., Tremonti, C., Kauffmann, G., Heckman, T., & Brinkmann, J. (2004). The physical properties of star-forming galaxies in the low-redshift Universe. *Monthly Notices of the Royal Astronomical Society*, 351(4), 1151–1179.

Bruzual, G. & Charlot, S. (2003a). Stellar population synthesis at the resolution of 2003. *Monthly Notices of the Royal Astronomical Society*, 344(4), 1000–1028.

Bruzual, G. & Charlot, S. (2003b). Stellar population synthesis at the resolution of 2003. *Monthly Notices of the Royal Astronomical Society*, 344(4), 1000–1028.

Bruzual A., G. (1983). Spectral evolution of galaxies. I - Early-type systems. *The Astrophysical Journal*, 273, 105.

Bryant, J. J., Owers, M. S., Robotham, A. S. G., Croom, S. M., Driver, S. P., Drinkwater, M. J., Lorente, N. P. F., Cortese, L., Scott, N., Colless, M., Schaefer, A., Taylor, E. N., Konstantopoulos, I. S., Allen, J. T., Baldry, I., Barnes, L., Bauer, A. E., Bland-Hawthorn, J., Bloom, J. V., Brooks, A. M., Brough, S., Cecil, G., Couch, W., Croton, D., Davies, R., Ellis, S., Fogarty, L. M. R., Foster, C., Glazebrook, K., Goodwin, M., Green, A., Gunawardhana, M. L., Hampton, E., Ho, I.-T., Hopkins, A. M., Kewley, L., Lawrence, J. S., Leon-Saval, S. G., Leslie, S., McElroy, R., Lewis, G., Liske, J., López-Sánchez, A. R., Mahajan, S., Medling, A. M., Metcalfe, N., Meyer, M., Mould, J., Obreschkow, D., O'Toole, S., Pracy, M., Richards, S. N., Shanks, T., Sharp, R., Sweet, S. M., Thomas, A. D., Tonini,

C., & Walcher, C. J. (2015). The SAMI Galaxy Survey: Instrument specification and target selection. *Monthly Notices of the Royal Astronomical Society*, 447(3), 2857–2879.

Bundy, K., Bershady, M. A., Law, D. R., Yan, R., Drory, N., MacDonald, N., Wake, D. A., Cherinka, B., Sánchez-Gallego, J. R., Weijmans, A.-M., Thomas, D., Tremonti, C., Masters, K., Coccato, L., Diamond-Stanic, A. M., Aragón-Salamanca, A., Avila-Reese, V., Badenes, C., Falcón-Barroso, J., Belfiore, F., Bizyaev, D., Blanc, G. A., Bland-Hawthorn, J., Blanton, M. R., Brownstein, J. R., Byler, N., Cappellari, M., Conroy, C., Dutton, A. A., Emsellem, E., Etherington, J., Frinchaboy, P. M., Fu, H., Gunn, J. E., Harding, P., Johnston, E. J., Kauffmann, G., Kinemuchi, K., Klaene, M. A., Knapen, J. H., Leauthaud, A., Li, C., Lin, L., Maiolino, R., Malanushenko, V., Malanushenko, E., Mao, S., Maraston, C., McDermid, R. M., Merrifield, M. R., Nichol, R. C., Oravetz, D., Pan, K., Parejko, J. K., Sanchez, S. F., Schlegel, D., Simmons, A., Steele, O., Steinmetz, M., Thanjavur, K., Thompson, B. A., Tinker, J. L., van den Bosch, R. C. E., Westfall, K. B., Wilkinson, D., Wright, S., Xiao, T., & Zhang, K. (2014). OVERVIEW OF THE SDSS-IV MaNGA SURVEY: MAPPING NEARBY GALAXIES AT APACHE POINT OBSERVATORY. *The Astrophysical Journal*, 798(1), 7.

Burgarella, D., Buat, V., Gruppioni, C., Cucciati, O., Heinis, S., Berta, S., Béthermin, M., Bock, J., Cooray, A., Dunlop, J. S., Farrah, D., Franceschini, A., Le Floc'h, E., Lutz, D., Magnelli, B., Nordon, R., Oliver, S. J., Page, M. J., Popesso, P., Pozzi, F., Riguccini, L., Vaccari, M., & Viero, M. (2013). *Herschel* PEP/HerMES: The redshift evolution ($0 \leq z \leq 4$) of dust attenuation and of the total (UV+IR) star formation rate density. *Astronomy & Astrophysics*, 554, A70.

Calzetti, D., Kennicutt, R. C., Engelbracht, C. W., Leitherer, C., Draine, B. T., Kewley, L., Moustakas, J., Sosey, M., Dale, D. A., Gordon, K. D., & others (2007). The calibration of mid-infrared star formation rate indicators. *The Astrophysical Journal*, 666(2), 870.

Chabrier, G. (2003). Galactic Stellar and Substellar Initial Mass Function. *Publications of the Astronomical Society of the Pacific*, 115, 763–795.

Chen, Y.-M., Kauffmann, G., Tremonti, C. A., White, S., Heckman, T. M., Kovač, K., Bundy, K., Chisholm, J., Maraston, C., Schneider, D. P., Bolton, A. S., Weaver, B. A., & Brinkmann, J. (2012). Evolution of the most massive galaxies to z= 0.6 - I. A new method for physical parameter estimation. *some journal name*, 421, 314–332.

Conroy, C. (2013). Modeling the panchromatic spectral energy distributions of galaxies. *arXiv preprint arXiv:1301.7095*.

Cooper, M. C., Newman, J. A., Madgwick, D. S., Gerke, B. F., Yan, R., & Davis, M. (2005). Measuring galaxy environments with deep redshift surveys. *The Astrophysical Journal*, 634(2), 833.

Crain, R. A., Schaye, J., Bower, R. G., Furlong, M., Schaller, M., Theuns, T., Dalla Vecchia, C., Frenk, C. S., McCarthy, I. G., Helly, J. C., Jenkins, A., Rosas-Guevara, Y. M., White, S. D. M., & Trayford, J. W. (2015). The EAGLE simulations of galaxy formation: calibration of subgrid physics and model variations. *some journal name*, 450, 1937–1961.

Creasey, P., Theuns, T., & Bower, R. G. (2013). How supernova explosions power galactic winds. *some journal name*, 429, 1922–1948.

da Cunha, E., Charlot, S., & Elbaz, D. (2008). A simple model to interpret the ultraviolet, optical and infrared emission from galaxies. *Monthly Notices of the Royal Astronomical Society*, 388(4), 1595–1617.

Davé, R., Thompson, R., & Hopkins, P. F. (2016). MUFASA: galaxy formation simulations with meshless hydrodynamics. *some journal name*, 462, 3265–3284.

Davis, M., Efstathiou, G., Frenk, C. S., & White, S. D. M. (1985). The evolution of large-scale structure in a universe dominated by cold dark matter. *some journal name*, 292, 371–394.

Draine, B. T. & Li, A. (2007). Infrared Emission from Interstellar Dust. IV. The Silicate-Graphite-PAH Model in the Post-Spitzer Era. *some journal name*, 657, 810–837.

Dressler, A. (1980). Galaxy morphology in rich clusters - Implications for the formation and evolution of galaxies. *The Astrophysical Journal*, 236, 351.

Drory, N., Bender, R., & Hopp, U. (2004). Comparing Spectroscopic and Photometric Stellar Mass Estimates. *some journal name*, 616, L103–L106.

Drory, N., MacDonald, N., Bershady, M. A., Bundy, K., Gunn, J., Law, D. R., Smith, M., Stoll, R., Tremonti, C. A., Wake, D. A., Yan, R., Weijmans, A. M., Byler, N., Cherinka, B., Cope, F., Eigenbrot, A., Harding, P., Holder, D., Huehnerhoff, J., Jaehnig, K., Jansen, T. C., Klaene, M., Paat, A. M., Percival, J., & Sayres, C. (2015). THE MANGA INTEGRAL FIELD UNIT FIBER FEED SYSTEM FOR THE SLOAN 2.5 M TELESCOPE. *The Astronomical Journal*, 149(2), 77.

Efstathiou, G., Ellis, R. S., & Peterson, B. A. (1988). Analysis of a complete galaxy redshift survey. II - The field-galaxy luminosity function. *some journal name*, 232, 431–461.

Eggen, O. J., Lynden-Bell, D., & Sandage, A. R. (1962). Evidence from the motions of old stars that the Galaxy collapsed. *some journal name*, 136, 748.

Ferland, G. J., Porter, R. L., van Hoof, P. A. M., Williams, R. J. R., Abel, N. P., Lykins, M. L., Shaw, G., Henney, W. J., & Stancil, P. C. (2013). The 2013 Release of Cloudy. *some journal name*, 49, 137–163.

Freeman, K. C. (1970). On the Disks of Spiral and so Galaxies. *The Astrophysical Journal*, 160, 811.

Gallazzi, A., Charlot, S., Brinchmann, J., White, S. D. M., & Tremonti, C. A. (2005). The ages and metallicities of galaxies in the local universe. *some journal name*, 362, 41–58.

Guth, A. H. (1981). Inflationary universe: A possible solution to the horizon and flatness problems. *Phys. Rev. D*, 23, 347–356.

Hopkins, P. F., Quataert, E., & Murray, N. (2012). Stellar feedback in galaxies and the origin of galaxy-scale winds. *some journal name*, 421, 3522–3537.

Hubble, E. (1929). A Relation between Distance and Radial Velocity among Extra-Galactic Nebulae. *Proceedings of the National Academy of Science*, 15, 168–173.

Ilbert, O., McCracken, H. J., Le Fèvre, O., Capak, P., Dunlop, J., Karim, A., Renzini, M. A., Caputi, K., Boissier, S., Arnouts, S., Aussel, H., Comparat, J., Guo, Q., Hudelot, P., Kartaltepe, J., Kneib, J. P., Krogager, J. K., Le Floc'h, E., Lilly, S., Mellier, Y., Milvang-Jensen, B., Moutard, T., Onodera, M., Richard, J., Salvato, M., Sanders, D. B., Scoville, N., Silverman, J. D., Taniguchi, Y., Tasca, L., Thomas, R., Toft, S., Tresse, L., Vergani, D., Wolk, M., & Zirm, A. (2013). Mass assembly in quiescent and star-forming galaxies since *z* â□□ 4 from UltraVISTA. *Astronomy & Astrophysics*, 556, A55.

Karim, A., Schinnerer, E., Martínez-Sansigre, A., Sargent, M. T., van der Wel, A., Rix, H.-W., Ilbert, O., Smolčić, V., Carilli, C., Pannella, M., Koekemoer, A. M., Bell, E. F., & Salvato, M. (2011). THE STAR FORMATION HISTORY OF MASS-SELECTED GALAXIES IN THE COSMOS FIELD. *The Astrophysical Journal*, 730(2), 61.

Kauffmann, G., Heckman, T. M., Simon White, D. M., Charlot, S., Tremonti, C., Brinchmann, J., Bruzual, G., Peng, E. W., Seibert, M., Bernardi, M., Blanton, M., Brinkmann, J., Castander, F., Csábai, I., Fukugita, M., Ivezic, Z., Munn, J. A., Nichol, R. C., Padmanabhan, N., Thakar, A. R., Weinberg, D. H., & York, D. (2003). Stellar masses and star formation histories for 10^5 galaxies from the Sloan Digital Sky Survey. *Monthly Notices of the Royal Astronomical Society*, 341(1), 33–53.

Kauffmann, G., White, S. D. M., Heckman, T. M., Ménard, B., Brinchmann, J., Charlot, S., Tremonti, C., & Brinkmann, J. (2004). The environmental dependence of the relations between stellar mass, structure, star formation and nuclear activity in galaxies: Galaxy structure, star formation and nuclear activity. *Monthly Notices of the Royal Astronomical Society*, 353(3), 713–731.

Kennicutt, R. C. & Evans, N. J. (2012). Star Formation in the Milky Way and Nearby Galaxies. *Annual Review of Astronomy and Astrophysics*, 50(1), 531–608.

Kennicutt, Jr., R. C. (1998). The Global Schmidt Law in Star-forming Galaxies. *some journal name*, 498, 541–552.

Kennicutt, Jr., R. C., Tamblyn, P., & Congdon, C. E. (1994). Past and future star formation in disk galaxies. *some journal name*, 435, 22–36.

Kroupa, P. (2001). On the variation of the initial mass function. *some journal name*, 322, 231–246.

Lee, J. C., Gil de Paz, A., Tremonti, C., Kennicutt, R. C., Salim, S., Bothwell, M., Calzetti, D., Dalcanton, J., Dale, D., Engelbracht, C., José G. Funes, S. J., Johnson, B., Sakai, S., Skillman, E., van Zee, L., Walter, F., & Weisz, D. (2009). COMPARISON OF Hα AND UV STAR FORMATION RATES IN THE LOCAL VOLUME: SYSTEMATIC DISCREPANCIES FOR DWARF GALAXIES. *The Astrophysical Journal*, 706(1), 599–613.

Leitherer, C. & Heckman, T. M. (1995). Synthetic properties of starburst galaxies. *some journal name*, 96, 9–38.

Leja, J., Johnson, B. D., Conroy, C., van Dokkum, P. G., & Byler, N. (2017). Deriving Physical Properties from Broadband Photometry with Prospector: Description of the Model and a Demonstration of its Accuracy Using 129 Galaxies in the Local Universe. *some journal name*, 837, 170.

Lewis, I., Balogh, M., De Propris, R., Couch, W., Bower, R., Offer, A., Bland-Hawthorn, J., Baldry, I. K., Baugh, C., Bridges, T., Cannon, R., Cole, S., Colless, M., Collins, C., Cross, N., Dalton, G., Driver, S. P., Efstathiou, G., Ellis, R. S., Frenk, C. S., Glazebrook, K., Hawkins, E., Jackson, C., Lahav, O., Lumsden, S., Maddox, S., Madgwick, D., Norberg, P., Peacock, J. A., Percival, W., Peterson, B. A., Sutherland, W., & Taylor, K. (2002). The 2dF Galaxy Redshift Survey: the environmental dependence of galaxy star formation rates near clusters. *some journal name*, 334, 673–683.

Madau, P. & Dickinson, M. (2014). Cosmic Star-Formation History. *Annual Review of Astronomy and Astrophysics*, 52(1), 415–486.

Madau, P., Pozzetti, L., & Dickinson, M. (1998). The Star Formation History of Field Galaxies. *some journal name*, 498, 106–116.

Moustakas, J., Coil, A. L., Aird, J., Blanton, M. R., Cool, R. J., Eisenstein, D. J., Mendez, A. J., Wong, K. C., Zhu, G., & Arnouts, S. (2013). PRIMUS: CONSTRAINTS ON STAR FORMATION QUENCHING AND GALAXY MERGING, AND THE EVOLUTION OF THE STELLAR MASS FUNCTION FROM z = 0-1. *The Astrophysical Journal*, 767(1), 50.

Muzzin, A., Marchesini, D., Stefanon, M., Franx, M., McCracken, H. J., Milvang-Jensen, B., Dunlop, J. S., Fynbo, J. P. U., Brammer, G., Labbé, I., & van Dokkum, P. G. (2013). THE EVOLUTION OF THE STELLAR MASS FUNCTIONS OF STAR-FORMING AND QUIESCENT GALAXIES TO z = 4 FROM THE COSMOS/UltraVISTA SURVEY. *The Astrophysical Journal*, 777(1), 18.

Muzzin, A., Marchesini, D., van Dokkum, P. G., Labbé, I., Kriek, M., & Franx, M. (2009). A Near-Infrared Spectroscopic Survey of K-Selected Galaxies at z~2.3: Comparison of Stellar Population Synthesis Codes and Constraints from the Rest-Frame NIR. *some journal name*, 701, 1839–1864.

Noeske, K. G., Weiner, B. J., Faber, S. M., Papovich, C., Koo, D. C., Somerville, R. S., Bundy, K., Conselice, C. J., Newman, J. A., Schiminovich, D., Le Floc'h, E., Coil, A. L., Rieke, G. H., Lotz, J. M., Primack, J. R., Barmby, P., Cooper, M. C., Davis, M., Ellis, R. S., Fazio, G. G., Guhathakurta, P., Huang, J., Kassin, S. A., Martin, D. C., Phillips, A. C., Rich, R. M., Small, T. A., Willmer, C. N. A., & Wilson, G. (2007). Star Formation in AEGIS Field Galaxies since z=1.1: The Dominance of Gradually Declining Star Formation, and the Main Sequence of Star-forming Galaxies. *some journal name*, 660, L43–L46.

Norberg, P., Baugh, C. M., Hawkins, E., Maddox, S., Madgwick, D., Lahav, O., Cole, S., Frenk, C. S., Baldry, I., Bland-Hawthorn, J., Bridges, T., Cannon, R., Colless, M., Collins, C., Couch, W., Dalton, G., De Propris, R., Driver, S. P., Efstathiou, G., Ellis, R. S., Glazebrook, K., Jackson, C., Lewis, I., Lumsden, S., Peacock, J. A., Peterson, B. A., Sutherland, W., & Taylor, K. (2002). The 2dF Galaxy Redshift Survey: the dependence of galaxy clustering on luminosity and spectral type. *some journal name*, 332, 827–838.

Papovich, C., Dickinson, M., & Ferguson, H. C. (2001). The Stellar Populations and Evolution of Lyman Break Galaxies. *some journal name*, 559, 620–653.

Park, C., Choi, Y.-Y., Vogeley, M. S., Gott, J. Richard, I., Blanton, M. R., & SDSS Collaboration (2007). Environmental Dependence of Properties of Galaxies in the Sloan Digital Sky Survey. *some journal name*, 658, 898–916.

Peebles, P. J. E. (1982). Large-scale background temperature and mass fluctuations due to scale-invariant primeval perturbations. *The Astrophysical Journal*, 263, L1.

Peng, Y.-j., Lilly, S. J., Kovač, K., Bolzonella, M., Pozzetti, L., Renzini, A., Zamorani, G., Ilbert, O., Knobel, C., Iovino, A., Maier, C., Cucciati, O., Tasca, L., Carollo, C. M., Silverman, J., Kampczyk, P., de Ravel, L., Sanders, D., Scoville, N., Contini, T., Mainieri, V., Scodeggio, M., Kneib, J.-P., Le Fèvre, O., Bardelli, S., Bongiorno, A., Caputi, K., Coppa, G., de la Torre, S., Franzetti, P., Garilli, B., Lamareille, F., Le Borgne, J.-F., Le Brun, V., Mignoli, M., Montero, E. P., Pello, R., Ricciardelli, E., Tanaka, M., Tresse, L., Vergani, D., Welikala, N., Zucca, E., Oesch, P., Abbas, U., Barnes, L., Bordoloi, R., Bottini, D., Cappi, A., Cassata, P., Cimatti, A., Fumana, M., Hasinger, G., Koekemoer, A., Leauthaud, A., Maccagni, D., Marinoni, C., McCracken, H., Memeo, P., Meneux, B., Nair, P., Porciani, C., Presotto, V., & Scaramella, R. (2010). MASS AND ENVIRONMENT AS DRIVERS OF GALAXY EVOLUTION IN SDSS AND zCOSMOS AND THE ORIGIN OF THE SCHECHTER FUNCTION. *The Astrophysical Journal*, 721(1), 193–221.

Penzias, A. A. & Wilson, R. W. (1965). A Measurement of Excess Antenna Temperature at 4080 Mc/s. *some journal name*, 142, 419–421.

Prugniel, P. & Soubiran, C. (2004). New release of the ELODIE library. *arXiv Astrophysics e-prints*.

Riess, A. G. et al. (1998). Observational evidence from supernovae for an accelerating universe and a cosmological constant. *Astron. J.*, 116, 1009–1038.

Roberts, M. S. & Haynes, M. P. (1994). Physical Parameters along the Hubble Sequence. *Annual Review of Astronomy and Astrophysics*, 32, 115–152.

Rubin, V. C., Thonnard, N., & Ford, Jr., W. K. (1980). Rotational properties of 21 SC galaxies with a large range of luminosities and radii, from NGC 4605 /R = 4kpc/ to UGC 2885 /R = 122 kpc/. *The Astrophysical Journal*, 238, 471.

Salim, S., Rich, R. M., Charlot, S., Brinchmann, J., Johnson, B. D., Schiminovich, D., Seibert, M., Mallery, R., Heckman, T. M., Forster, K., & others (2007a). UV Star Formation Rates in the Local Universe. *The Astrophysical Journal Supplement Series*, 173(2), 267.

Salim, S., Rich, R. M., Charlot, S., Brinchmann, J., Johnson, B. D., Schiminovich, D., Seibert, M., Mallery, R., Heckman, T. M., Forster, K., & others (2007b). UV Star Formation Rates in the Local Universe. *The Astrophysical Journal Supplement Series*, 173(2), 267.

Salpeter, E. E. (1955). The Luminosity Function and Stellar Evolution. *some journal name*, 121, 161.

Sánchez, S. F., Kennicutt, R. C., Gil de Paz, A., van de Ven, G., Vílchez, J. M., Wisotzki, L., Walcher, C. J., Mast, D., Aguerri, J. A. L., Albiol-Pérez, S., Alonso-Herrero, A., Alves, J., Bakos, J., Bartáková, T., Bland-Hawthorn, J., Boselli, A., Bomans, D. J., Castillo-Morales, A., Cortijo-Ferrero, C., de Lorenzo-Cáceres, A., del Olmo, A., Dettmar, R.-J., Díaz, A., Ellis, S., Falcón-Barroso, J., Flores, H., Gallazzi, A., García-Lorenzo, B., González Delgado, R., Gruel, N., Haines, T., Hao, C., Husemann, B., Iglésias-Páramo, J., Jahnke, K., Johnson, B., Jungwiert, B., Kalinova, V., Kehrig, C., Kupko, D., López-Sánchez, A. R., Lyubenova, M., Marino, R. A., Mármol-Queraltó, E., Márquez, I., Masegosa, J., Meidt, S., Mendez-Abreu, J., Monreal-Ibero, A., Montijo, C., Mourão, A. M., Palacios-Navarro, G., Papaderos, P., Pasquali, A., Peletier, R., Pérez, E., Pérez, I., Quirrenbach, A., Relaño, M., Rosales-Ortega, F. F., Roth, M. M., Ruiz-Lara, T., Sánchez-Blázquez, P., Sengupta, C., Singh, R., Stanishev, V., Trager, S. C., Vazdekis, A., Viironen, K., Wild, V., Zibetti, S., & Ziegler, B. (2012). CALIFA, the Calar Alto Legacy Integral Field Area survey: I. Survey presentation⋆. *Astronomy & Astrophysics*, 538, A8.

Sánchez-Blázquez, P., Peletier, R. F., Jiménez-Vicente, J., Cardiel, N., Cenarro, A. J., Falcón-Barroso, J., Gorgas, J., Selam, S., & Vazdekis, A. (2006). Medium-resolution Isaac Newton Telescope library of empirical spectra. *some journal name*, 371, 703–718.

Schmidt, M. (1959). The Rate of Star Formation. *some journal name*, 129, 243.

Sijacki, D., Vogelsberger, M., Genel, S., Springel, V., Torrey, P., Snyder, G. F., Nelson, D., & Hernquist, L. (2015). The Illustris simulation: the evolving population of black holes across cosmic time. *some journal name*, 452, 575–596.

Smee, S. A., Gunn, J. E., Uomoto, A., Roe, N., Schlegel, D., Rockosi, C. M., Carr, M. A., Leger, F., Dawson, K. S., Olmstead, M. D., Brinkmann, J., Owen, R., Barkhouser, R. H., Honscheid, K., Harding, P., Long, D., Lupton, R. H., Loomis, C., Anderson, L., Annis, J., Bernardi, M., Bhardwaj, V., Bizyaev, D., Bolton, A. S., Brewington, H., Briggs, J. W., Burles, S., Burns, J. G., Castander, F. J., Connolly, A., Davenport, J. R. A., Ebelke, G., Epps, H., Feldman, P. D., Friedman, S. D., Frieman, J., Heckman, T., Hull, C. L., Knapp, G. R., Lawrence, D. M., Loveday, J., Mannery, E. J., Malanushenko, E., Malanushenko, V., Merrelli, A. J., Muna, D., Newman, P. R., Nichol, R. C., Oravetz, D., Pan, K., Pope, A. C., Ricketts, P. G., Shelden, A., Sandford, D., Siegmund, W., Simmons, A., Smith, D. S., Snedden, S., Schneider, D. P., SubbaRao, M., Tremonti, C., Waddell, P., & York, D. G. (2013). THE MULTI-OBJECT, FIBER-FED SPECTROGRAPHS FOR THE

SLOAN DIGITAL SKY SURVEY AND THE BARYON OSCILLATION SPECTROSCOPIC SURVEY. *The Astronomical Journal*, 146(2), 32.

Smoot, G. F., Bennett, C. L., Kogut, A., Wright, E. L., Aymon, J., Boggess, N. W., Cheng, E. S., de Amici, G., Gulkis, S., Hauser, M. G., Hinshaw, G., Jackson, P. D., Janssen, M., Kaita, E., Kelsall, T., Keegstra, P., Lineweaver, C., Loewenstein, K., Lubin, P., Mather, J., Meyer, S. S., Moseley, S. H., Murdock, T., Rokke, L., Silverberg, R. F., Tenorio, L., Weiss, R., & Wilkinson, D. T. (1992). Structure in the COBE Differential Microwave Radiometer First-Year Maps. *some journal name*, 396, L1.

Somerville, R. S. & Davé, R. (2015). Physical Models of Galaxy Formation in a Cosmological Framework. *Annual Review of Astronomy and Astrophysics*, 53, 51–113.

Spinrad, H. & Taylor, B. J. (1971). The Stellar Content of the Nuclei of Nearby Galaxies. I. M31, M32, and M81. *some journal name*, 22, 445.

Strateva, I., Ivezić, Ž., Knapp, G. R., Narayanan, V. K., Strauss, M. A., Gunn, J. E., Lupton, R. H., Schlegel, D., Bahcall, N. A., Brinkmann, J., Brunner, R. J., Budavári, T., Csabai, I., Castander, F. J., Doi, M., Fukugita, M., Győry, Z., Hamabe, M., Hennessy, G., Ichikawa, T., Kunszt, P. Z., Lamb, D. Q., McKay, T. A., Okamura, S., Racusin, J., Sekiguchi, M., Schneider, D. P., Shimasaku, K., & York, D. (2001). Color Separation of Galaxy Types in the Sloan Digital Sky Survey Imaging Data. *some journal name*, 122, 1861–1874.

Tomczak, A. R., Quadri, R. F., Tran, K.-V. H., Labbé, I., Straatman, C. M. S., Papovich, C., Glazebrook, K., Allen, R., Brammer, G. B., Kacprzak, G. G., Kawinwanichakij, L., Kelson, D. D., McCarthy, P. J., Mehrtens, N., Monson, A. J., Persson, S. E., Spitler, L. R., Tilvi, V., & van Dokkum, P. (2014). GALAXY STELLAR MASS FUNCTIONS FROM ZFOURGE/CANDELS: AN EXCESS OF LOW-MASS GALAXIES SINCE $z = 2$ AND THE RAPID BUILDUP OF QUIESCENT GALAXIES. *The Astrophysical Journal*, 783(2), 85.

Tremonti, C. A., Heckman, T. M., Kauffmann, G., Brinchmann, J., Charlot, S., White, S. D. M., Seibert, M., Peng, E. W., Schlegel, D. J., Uomoto, A., Fukugita, M., & Brinkmann, J. (2004). The Origin of the Mass-Metallicity Relation: Insights from 53,000 Star-forming Galaxies in the Sloan Digital Sky Survey. *The Astrophysical Journal*, 613(2), 898–913.

Worthey, G. (1994). Comprehensive stellar population models and the disentanglement of age and metallicity effects. *The Astrophysical Journal Supplement Series*, 95, 107.

Wright, E. L., Eisenhardt, P. R. M., Mainzer, A. K., Ressler, M. E., Cutri, R. M., Jarrett, T., Kirkpatrick, J. D., Padgett, D., McMillan, R. S., Skrutskie, M., Stanford, S. A., Cohen, M., Walker, R. G., Mather, J. C., Leisawitz, D., Gautier, T. N., McLean, I., Benford, D., Lonsdale, C. J., Blain, A., Mendez, B., Irace, W. R., Duval, V., Liu, F., Royer, D., Heinrichsen, I., Howard, J., Shannon, M., Kendall, M., Walsh, A. L., Larsen, M., Cardon, J. G., Schick, S., Schwalm, M., Abid, M., Fabinsky, B., Naes, L., & Tsai, C.-W. (2010). THE WIDE-FIELD INFRARED SURVEY EXPLORER (WISE): MISSION DESCRIPTION AND INITIAL ON-ORBIT PERFORMANCE. *The Astronomical Journal*, 140(6), 1868–1881.

Wyder, T. K., Martin, D. C., Schiminovich, D., Seibert, M., Budavari, T., Treyer, M. A., Barlow, T. A., Forster, K., Friedman, P. G., Morrissey, P., Neff, S. G., Small, T., Bianchi, L., Donas, J., Heckman, T. M., Lee, Y.-W., Madore, B. F., Milliard, B., Rich, R. M., Szalay, A. S., Welsh, B. Y., & Yi, S. K. (2007). The UV-Optical Galaxy Color-Magnitude Diagram. I. Basic Properties. *The Astrophysical Journal Supplement Series*, 173(2), 293–314.

Yan, R., Chen, Y., Lazarz, D., Bizyaev, D., Maraston, C., Stringfellow, G. S., McCarthy, K., Meneses-Goytia, S., Law, D. R., Thomas, D., Falcon Barroso, J., Sánchez-Gallego, J. R., Schlafly, E., Zheng, Z., Argudo-Fernández, M., Beaton, R. L., Beers, T. C., Bershady, M., Blanton, M. R., Brownstein, J., Bundy, K., Chambers, K. C., Cherinka, B., De Lee, N., Drory, N., Galbany, L., Holtzman, J., Imig, J., Kaiser, N., Kinemuchi, K., Liu, C., Luo, A.-L., Magnier, E., Majewski, S., Nair, P., Oravetz, A., Oravetz, D., Pan, K., Sobeck, J., Stassun, K., Talbot, M., Tremonti, C., Waters, C., Weijmans, A.-M., Wilhelm, R., Zasowski, G., Zhao, G., & Zhao, Y.-H. (2018). SDSS-IV MaStar – A Large and Comprehensive Empirical Stellar Spectral Library: First Release. *arXiv e-prints*, (pp. arXiv:1812.02745).

Zibetti, S., Charlot, S., & Rix, H.-W. (2009). Resolved stellar mass maps of galaxies - I. Method and implications for global mass estimates. *some journal name*, 400, 1181–1198.

Zwicky, F. (1937). On the Masses of Nebulae and of Clusters of Nebulae. *some journal name*, 86, 217.